ADDIS ABABA UNIVERSITY
SCHOOL OF GRADUATE STUDIES

APPLICATION OF INTEGRATED GEOPHYSICAL TECHNIQUES TO MAP GROUNDWATER POTENTIAL ZONES AND GEOLOGICAL STRUCTURES AT GELCHET AREA, BORENA ZONE, SOUTH ETHIOPIA

BY

MULUGETA CHANIE FENTA

A THESIS SUBMITTED TO THE SCHOOL OF GRADUATE STUDIES OF ADDIS ABABA UNIVERSITY IN PARTIAL FULFILMENT OF THE REQUIREMENTS FOR THE DEGREE OF MASTER OF SCIENCE IN EXPLORATION GEOPHYSICS

FEBRUARY,2011

Addis Ababa University
School of Graduate Studies
Department of Earth Sciences

Application of integrated geophysical techniques to map groundwater potential zones and geological structures at Gelchet Area, Borena Zone, South Ethiopia.

By

Mulugeta Chanie Fenta

Approved by board of examiners:

Dr. Tigistu Haile	Signature _____
Chairman, Department of Earth sciences	
Dr. Elias Lewi	Signature_____
Advisor	
Dr. Tigistu Haile	Signature_____
Co-advisor	
Dr._____	Signature _____
Internal Examiner	
Dr. _____	Signature _____
External Examiner	

ACKNOWLEDGEMENT

First of all, I would like to thank the almighty God for everything He does in my life.

I have nothing to say to my advisor Dr. Elias Lewi for his crucial comments and sound suggestions that he gave me in order to accomplish this thesis successfully. During the time that I engaged in this work, he acted like not only my advisor but also like my father and colleague. I thank you for everything that you did for me.

I would like to express my grateful thank to my co-advisor Dr.Tigistu Haile for his unreserved support, suggestions and crucial comments to accomplish this work successfully. I have great respect in my life for you due to your rational and enthusiasm behavior to help others.

I would like to say thank you for Dr.Shimeles Fisseha who gave me valuable references, suggestions and the chance to collect the gravity and GPS data which is the cause to do my thesis.

I am also thankful to the Oromia water works design and supervision enterprise office where I got the resistivity data, lithologic logs and geological reports of the study area, Institute of geophysics, space science and astronomy, Department of Earth Sciences and Geological survey of Ethiopia for their support and encouragement.

My thanks go also to my friends Elias Abebe,Yelebe Birhanu, Tagel Assefa and Dilbi Siraj for their support to use different softwares to process the geophysical data.

Last but not least, I thank you to all my family and friends for their support and encouragement during the period of this work.

ABSTRACT

Integrated geophysical survey using vertical electrical sounding (VES) and gravity (with differential GPS) methods were conducted to investigate groundwater potential zones and geological structures at Gelchet area, Borena zone, South Ethiopia. The main objectives of this study were to map groundwater potential zones and determine depth to the basement. Geologically, the area is located within the Cenozoic volcanic plain that followed by Precambrian crystalline basement rocks to the southeast of main Ethiopian rift.

The data acquired from twenty eight (28) VES points using Schlumberger electrode array with maximum half current electrode spacing (AB/2=1000m) and 115 gravity points (supported by high accuracy height control from GPS method) were interpreted both qualitatively and quantitatively in order to understand the local geology and identify aquifer bearing horizons. The qualitative analysis of VES data were performed by using pseudodepth sections and different apparent resistivity maps. Similarly, the qualitative interpretations of gravity data were performed by using gravity profile plots and different gravity anomaly maps. Finally, the overall qualitative interpretation was done by integrating all the above results together with the geologic , topographic maps and borehole information. As a result of this, geologic structures and groundwater potential zones are identified and drilling sites are recommended.

The quantitative interpretations of the VES data were conducted by modeling the VES data using Resix-Ip and WinResist modeling softwares and constructing geoelectric sections along selected survey lines, using the result from individual VES point interpretations. The depth and lithologic units from the boreholes were used to fix parameters during the modeling of VES data. The information from the VES data and the boreholes were used to constrain the depth information in the gravity modeling which were conducted on two survey lines. The VES results of the data revealed four main geoelectric layers which differ in degree of weathering, fracturing, composition and depth of burial. The geoelectric sections enabled to identify the overburden thickness and the depth to the aquifer along survey lines whereas the gravity model helped to identify basement undulation in places where there is no VES data. Moreover, the vertical electrical sounding survey helped to identify groundwater potential areas and determine the depth to the aquifer whereas the gravity survey helped to map the basement topography and identify places having high groundwater reservoir potential.

TABLE OF CONTENETS **PAGE**

LIST OF FIGURES PAGE

LIST OF TABLES PAGE

ACRONYMS

1D-One Dimension

2D-Two Dimension

3D-Three Dimension

BTW7-Borena Test well 7

DGPS-Differential Global Positioning System

GMT-Generic mapping tool

GPS-Global Positioning System

GPW2-Gelchet Production Well 2

GPW3-Gelchet Production Well 3

GPW4-Gelchet Production Well 4

GPW6-Gelchet Production Well 6

GRS-Geodetic References System

GW1-Gelchet Well 1

GW2-Gechet Well 2

GW3--Gelchet Well 3

GW4- Gelchet Well 4

GW5-Gelchet Well 5

IGSN-International Gravity Standardization Net

ITRF-International Terrestrial References Frame

OWWDSE-Oromia Water Works Design and Supervision enterprise

RINEX-Receiver Independent Exchange Format

RMS-Root Mean Square

SWL-Static Water Level

TGO-Trimble Geomantic Offices

UNAVCO-University of NAVASTAR Consortium

UTM-Universal Transverse Mercator

VES-Vertical Electrical Sounding

WGS-World Geodetic System

CHAPTER ONE

INTRODUCTION

1.1 General

Water is one of the basic needs to sustain life. Without it survival is limited to very few days. Living things such as humans, animals and plants are dependent on water. Human need water for several functions such as agriculture, power generation, domestic use and as a basic part of daily life. Human beings can exist without food for weeks but can't exist without water for more than a few days. Therefore, we can say that water is the elixir of life. This intimate relationship between water and life plays a great role to establish a permanent community and its way of utilization determines the developmental level of a country.

The largest amount of water on earth (97.2 %) is contained in the oceans and seas as a saline or salty water but only small amount of it (2.8 %) exist as fresh water on land. This fresh water found on land is distributed as Ice caps and glaciers (76.43 %), groundwater and soil moisture (21.96 %), fresh-water lakes (0.32%), saline-lakes (0.29 %) and very small amount of it as streams channels (0.004 %) (Fetter, C.W., 2001). The amount of fresh water which is available for domestic, industrial and agriculture purposes is very limited as compared to the total volume of water on the planet earth. However, it is found relatively in large amount next to ice caps and glaciers, requires less expense to purification and transport, occurs in places where there is scarce amount of surface water supply and others made it to be vital source for drinking, domestic and livestock use for rural population including Ethiopia. Due to the above reasons, the search for ground water is vital as an immediate and sustainable solution to alleviate the scarcity of water for drinking and other domestic uses in Ethiopia.

The shallow subsurface of the earth is an extremely important zone that yields much of our water resources, support our agriculture and ecosystem. Population growth and economical progress required greater volumes of fresh water and at the same time emphasizes the need to protect and sustain known supplies and resources (Ledo, L., 2007).

Since there is no any river, stream or spring in the study area, hand dug wells and drilled boreholes are the only sources of drinking water for the people to have permanent settlement.

Therefore, the major objective of this study is to identify potential areas for extraction of groundwater resources and minimize the risk of sinking boreholes at inappropriate areas.

The people who live in the study area are mainly nomads except those found in near towns of Yabelo, Mega, Dubuluk and Teltle. They travel from place to place to look for water and pasture for their cattle. Though the availability of constant water supply is one of the major issues that dictate the settlement of the pastoralist in the area, it is not enough by itself for constant settlement due to the demand for enough pasture. Therefore, the detailed geophysical study for groundwater exploration is crucial thing for the area.

1.1.1 Location and Accessibility

Gelchet is located in the southwestern part of the Borena zone, Oromia national regional state, South Ethiopia. It is part of the vast tract of Borena land located to the west of Yabello-Moyale main road along the Ethio-Kenyan boarder in the Dire woreda. The universal transverse Mercator (UTM) coordinate which bounds the area is 353400-365500 Easting , 503000-513000 Northing and 1053.26- 1132.452m height from the 1984 World Geodetic System (WGS84) reference ellipsoid. Figure 1.1 shows the location of the study area including its topography in relation to the nearby surrounding. The 90 m interval girded XYZ Shuttle Radar Topographic Mission (SRTM) satellite data was used by the generic mapping tool (GMT) to produce the location map of study area.

The land distance to the area is 670 km south of Addis Ababa and has an air distance of around 80 km from Northern Kenya border. It can be accessed by two alternative roads along the asphalt road from Addis Ababa to the border town of Moyale via towns of Hawasa, Dilla and zonal town Yabello or Addis Ababa to Arba-Minch ,Yabello and finally to Gelchet.

The first alternative route to the area is using the Addis Ababa-Yabello main asphalt road which is 570km followed by the 20km drive along Yabello-Moyale main asphalt road and finally 80km dry weather road that traverse towards west.

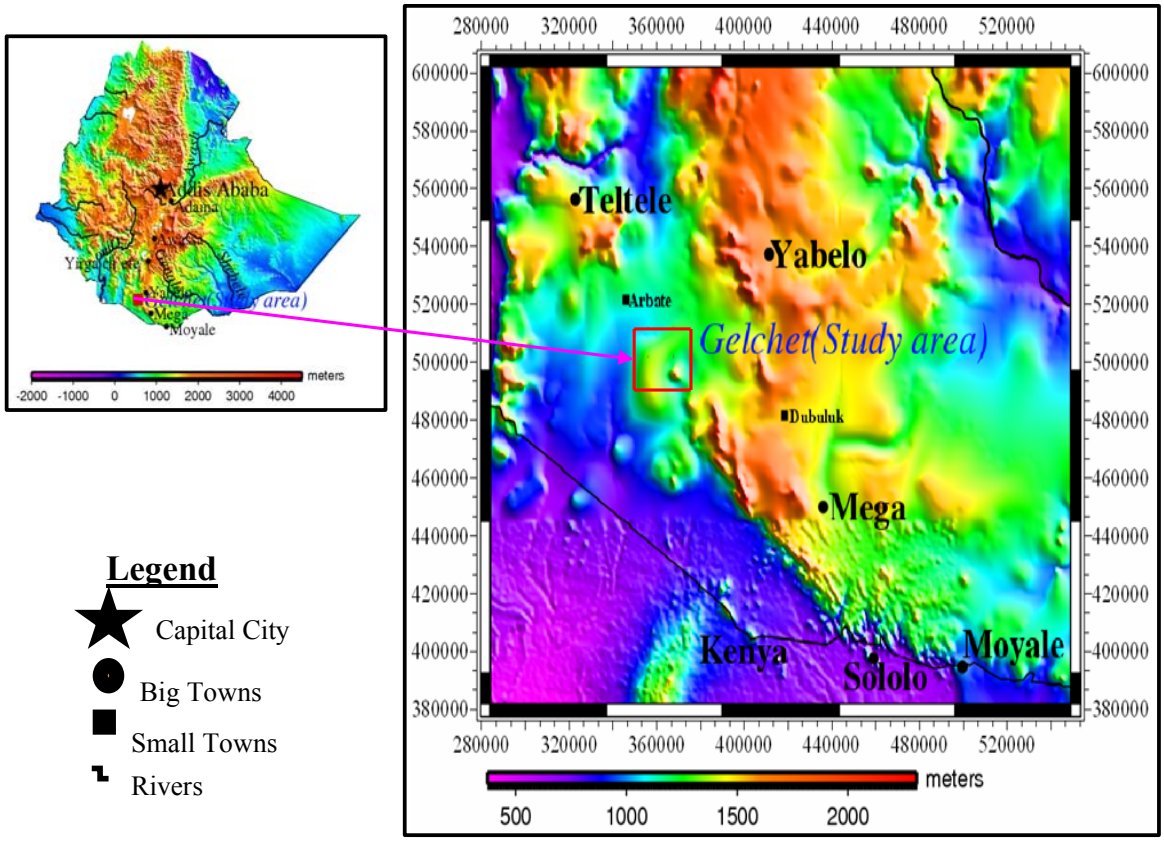

Figure 1.1 Location map of the study area.

There are no any infrastructures like electricity, telephone, banking, health sectors and postal services in the study area. As a result of this, one needs to travel to Yabello town which is 100km northeast of the study area to access the above mentioned infrastructural facilities.

1.1.2 Climate and Vegetation

The climatic condition of the area is similar to the other vast tract land of Borena zone and it is characterized by arid to semi-arid climatic conditions with two rainy seasons. These are from March to May and September to November, but rarely with little rainfall from June to August whereas December and January are the hottest months (Awoke, H. and Hailu, F., 2007). The main rainy season in the area is March, May and April whereas the short rainy season occurs in September, October and November. Even though the mean monthly maximum and minimum temperature and annual precipitation data for the locality is not available for this work, verbal communication revealed that the rainfall amount is better than Yabello town which has an annual precipitation of 630mm. Since most of the area is plain land, the effect of runoff is not

significantly seen in the area. Most of the drilled holes after this and other similar studies in the area are productive. However, some studies (Belete *et al* 2000) claimed that the evaporation of the Borena land including the study area exceeds precipitation and has rain fall deficit to replenish the groundwater including the study area.

The vegetation cover of the area is mostly continuous, dense and tall grass with thorny shrubs, wild seasonal, and scattered small trees. There is no any agricultural works in the area by the pastoralist.

1.2 Geology of the study area

1.2.1 Regional Geology

The geological setting of the vast tract of Borena land in areas south west of Yabello-Moyale main road and North of the Ethio-Kenyan border is found partly with in the east African orogen, close to and partly in the broadly rifted zone of East African Rift system in the South Ethiopia. The geology of this area consists of two major groups of rocks named as Precambrian crystalline basement complex, Cenozoic volcanic and quaternary superficial deposits. The Precambrian crystalline Basement rocks which are exposed in the northeastern and southwestern parts of the area are comprise of high-grade gneisses, schist, weakly to moderately metamorphosed volcano-sedimentary rocks.

The older metamorphic complex is formed from various gneiss and granulites invariably intruded by pre- and post intrusive and younger plutonic rocks. The Precambrian rocks of the area exhibit similar lithologic association, structural features and grade of metamorphism characteristic to both Mozambique Belt and Arabian Nubian Shield to the south and north respectively (Aweke, H. and Hailu, F., 2007).

The Cenozoic volcanic forms the mountain ridges of the western and low-laying plain areas in the central and southern parts whereas the eastern elevated grounds were formed from the basement rocks. The greater percentage of the area except the margins is characterized by subdued grounds of volcanic plains underlain by hundreds of meters thick basalt flows with fine to coarse columnar structure. Being bounded by the Ethiopia rift in northeast to southwest and its resulting volcanic mountains from west, the Borena land which are covered by the volcanic

plains are crossed by two rift systems called Rirriba rift and Mega rift systems. The Rirriba Rift has north-south trend whereas Mega rift system has northwest-southeast trend.

1.2.2 The Geological Setting of Gelchet Area.

Geologically the Gelchet area (including the area where geophysical survey was conducted) lies on volcanic plains underlain by basement rocks similar to the other Borena lands. The volcanic rocks are observed as boulders in the area. The exposed basaltic formation over the area is highly vesicular basalt which is confirmed from the drilled well lithology. The part of the basement rock which lies below the volcanic rocks is weathered and fractured with different degrees at different places. In the drilled wells, the weathered part of basement rock is fully penetrated and massive part of the basement rock is partially penetrated.

The observed and identified geological make up of the area as it was mapped and described by Oromia water works design and supervision Enterprise geological report (OWWDSE,2008), is arranged from bottom to top as: Banded gneiss, Quaternary vesicular basalt, Quaternary Scoraceous basalt, Scoria, Elluvial and Alluvial deposits. The areal coverage of these rocks are shown in geological map of the Gelchet area (Figure 1.2) and their descriptions are given below.

A) Banded Gneiss

It is composed of mainly a suite of quartzo-feldspathic rock that are variably inter layered with mafic gneisses, and intercalated with sporadic schists. A small outcrop of this unit is present on the southern part of the area which is a continuation of the Kenchero Gneiss mountain outside but near to the study area, covering less than 1% of the total mapped area.

B) Quaternary Vesicular Basalt

It is exposed in the western and eastern parts of the area which predominantly covers 76 % of the total area. The outcrops of this rock exhibit highly fractured basalt with relatively coarse fragments, whose surfaces are covered by carbonaceous coatings. The inside of some vesicular fragments looks like a bee-net with charcoal like surfacial appearance.

Generally it is gray to dark gray, fine to medium grained commonly very fresh and young looking. At some places where the vesicles are filled with secondary minerals such as quartz, calcite, and zeolites, the rock has amygdaloidal appearance.

C) Quaternary Scoraceous Basalt

The outcrop nature of this unit looks like that of scoria, but the abundance of scoria is insignificant compared to scoriaceous basalt and covers less than 1% of the total surface area which is very small area coverage. The outcrops of this rock are not extensive and continuous rather it is observed as scattered boulders, cobbles and some pebbles of scoriaceous basalt together with vesicular basalt.

Megascopically the scoriaceous basalt is reddish brown, massive and dense rock exposed in the form of floats. The denseness of the rock indicates that it is made up of closely packed crystalline minerals, unlike the light scoria that is predominantly made up of glass. The reddish brown color is believed to be the result of oxidation of mafic minerals like olivine and pyroxene.

D) Scoria

The out crops of this unit are observed at the northern part, in the form of sub-rounded body and covers 0.14 % of the total mapped area. The scoria is reddish brown, grayish black and it is formed of loosely packed/agglutinated cobble, gravel, and lazily sized cinder which in some cases show graded bedding. The scoria is predominantly made up of glass but the presence of small percentages of plagioclase and mafic minerals to be altered to Fe-oxides which give its characteristic reddish brown color. It also consists of small amounts of denser scoriaceous basalt.

E) Elluvial Deposit

The outcrops of this unit observed in the north-western part of the area which covers 9.24 % of the total mapped area. It consists of residual or short transported soils such as sand, silt, and gravel in which the silt sized particles predominate and covers flat or gently sloping topography by increasing in thickens towards west corresponding to the declining topography. From the

mineralogical composition of the elluvial deposit, it is expected to be formed as a result of the weathering and disintegration of the basalt so that it has mostly darker colored and the constituent minerals are mafic minerals, feldspar, and rock fragments with subordinate magnetite, and mica.

F) Alluvium

The alluvial deposit, which covers 14 % of the totally mapped area, is exposed occupying stream beds, flood plains, and stream banks. It is mainly composed of sand, silt, and clay in various proportions with some pebbles and cobbles with color varying from grayish white through reddish brown and black. The constituent minerals of the sand and silt are chiefly quartz, feldspar, and rounded to sub-rounded rock fragments with subordinate magnetite, biotite and white mica. The alluvial deposits of the flood plains are specifically black consisting of clay or Silty clay and the larger fragments being left behind earlier due to the low energy of the flood since it is flowing over wide area.

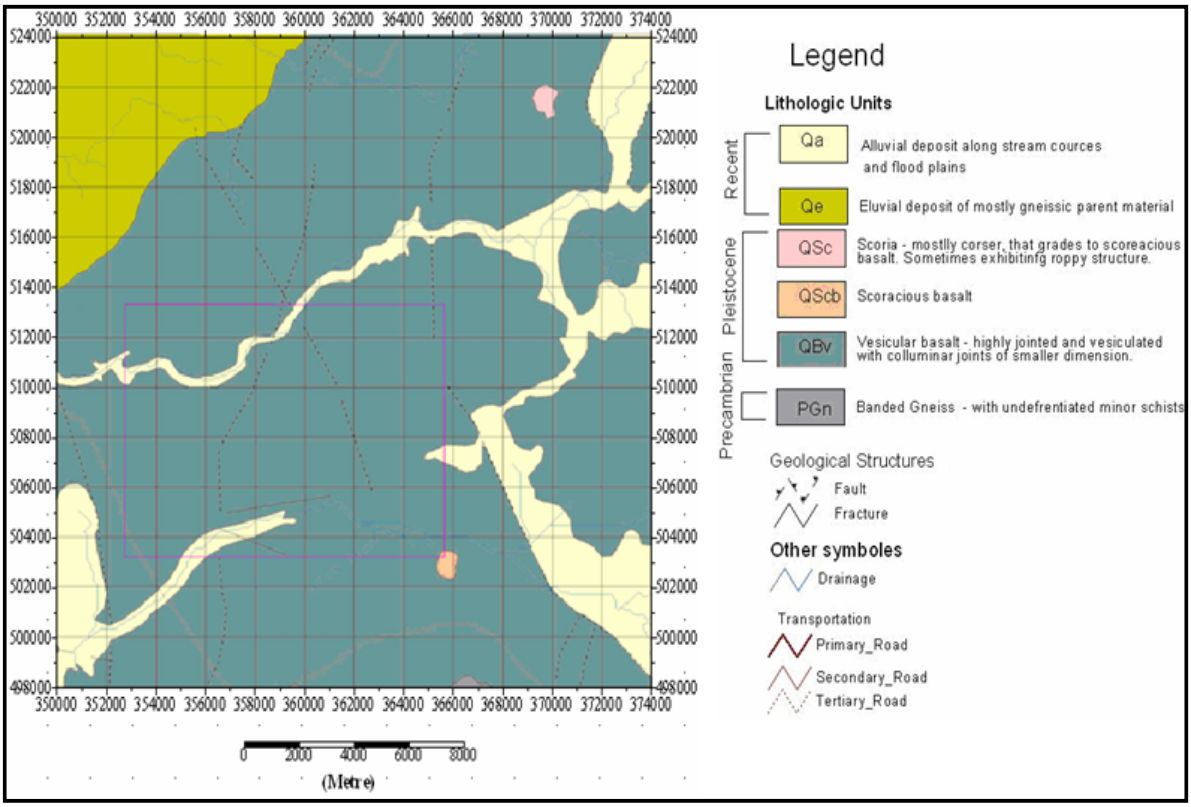

Figure 1. 2 Geological map of Gelchet area (OWWDSE, 2008)

As shown in the Figure above, the survey area is found in the Gelchet area but didn't include the whole types of rocks shown in the Gelchet area rather it is mainly covered by quaternary vesicular basalts and quaternary alluvial deposits. There is also some quaternary scoriaceous basalt shown in the southeast corner of the area which covers very small amount of the survey area.

1.3 Hydrogeology

The different in mineralogy, texture and structure of the volcanic rocks leads to have variable water bearing capacity. Groundwater circulation and storage in the volcanic rocks depend on the type of porosity and permeability formed during and after the rock formation (Alemayehu, T., 2006). The occurrence of groundwater in the basement and volcanic rocks is governed by the volume and behavior of faults, fissures, flow breccias, porous zones between successive lava beds, cracks and joints (Belete *et al* 2000). The primary porosities such as vesicles and flow contacts or interflow spaces in the volcanic rocks are also factors that determine the water bearing capacity in addition to the aforementioned secondary porosities. The groundwater occurrences in the metamorphic rocks are in the fractured and weathered parts of the rock. In the case of volcanic rocks, the sizes of fractures are the predominant factors whereas for metamorphic rocks; the storage capacity is determined by the type of weathering products and the thickness of the consequent weathered layer. Metamorphic rocks are mostly impervious and serve as aquicludes and the only water bearing zones in many of them are the upper loose and weathered parts. Hence metamorphic rocks are characterized by secondary permeability which decreases with depth, the groundwater yield to wells decrease rapidly as depth increase.

The weathered and fractured vesicular basalt rocks, the contact between the fractured and massive basalts and the upper weathered and fractured part of basement rock that lies below the volcanic rock are the potential aquifers for the drilled wells in the area due to their high permeability and porosity for the percolation of groundwater to the saturated zone.
The drilled boreholes information in the study area is given in Table 1.1 below.

Table 1.1 Borehole information in the study area.

Borehole code	UTM Coordinates(m)			Depth (m)	Water strike (m) (top of aquifer)	Static water level (SWL) (m)	Pumping test Yield(l/s)	Draw dawn(m) during pumping test
	X	Y	Z					
BTW7	361304	509658	1137	213	157	131	>5.6	on progress
GPW2	362521	507901	1136	204	160	132	3	on progress
GPW3	363415	511851	1148	244	148	138.5	3	33.74
GPW4	358421	510878	1130	201	on progress	on progress	Dry	on progress
GPW6	358378	511796	1091	143	on progress	on progress	Dry	on progress
GW1	360826	505258	1120	185	128	112	>17	on progress
GW2	362519	506349	1130	181	138	124.3	>15	on progress
GW3	358637	506621	1132	204	150	129	on progress	on progress
GW4	361707	505679	1125	189	133	120	on progress	on progress
GW5	358825	504597	1112	138	on progress	on progress	on progress	on progress

1.4 Previous Works

Several geological, hydrogeological, geophysical and engineering geological studies have been conducted in Borena zone which includes the study area for various purposes. The results of

these studies conducted by different authors with different scale includes ; geology of Ethiopia, explanatory notes to geological map of Ethiopia (Kazmin, V,. 1972); geology of Yabelo map sheet, NB 37-14(Awoke, H. and Hailu, F., 2007); Borena groundwater project, detailed geological report (OWWDSE, 2008); hydrogeological, geophysical and engineering geological investigation of yabelo map sheet, NB 37-14 (Belete *et al* 2000).

1.5 Objectives of the study

General Objectives

- The main objective of the VES survey is to look for groundwater potential areas and determine the depth at which the aquifers are located.
- The objective of the gravity survey is to map the basement topography and to asses places having high groundwater reservoir potential.

Specific Objectives

- To determine depth to the basement along the profiles
- To identify the major subsurface geological units
- To continuously map lateral contacts between geologic units differing in mass and density.
- To identify geologically weak zones that serve as a conduit for groundwater movement.
- To determine the depth to groundwater table and to locate potential drilling sites for the extraction of groundwater.

CHAPTER TWO

THEORY OF GEOPHYSICAL METHODS

2.1 Introduction

Geophysical techniques used in this study include electrical resistivity and gravity methods, assisted by Differential Global Positioning system (DGPS) techniques. The resistivity method is used for detecting groundwater presence and differentiating subsurface layers where as the gravity method is used in groundwater exploration to detect the structural trends controlling the geometry of the groundwater aquifer (Sultan *et al* 2009). From the electrical resistivity method, one can deduce hydrogeological information such as the availability of water and water quality whereas the gravity method is used to get information about the presence of structures such as faults, folds, aquifer bounding structures as well as to estimate depth to the basement and their shape, which are important information to assess the groundwater potential zones in the area.

2.2 Theory of Electrical Resistivity Method

2.2.1 General

Electrical resistivity methods have been used in a number of groundwater exploration surveys when the resistivities of the rocks are needed to be inferred. The resistivity of shallow subsurface of the Earth which yields much of our groundwater resources depends on the clay content, formation porosity, amount of water in the rock and the salinity of the water in the rocks. The electrical conductivity of these rocks will increase when they are saturated well with water compared to unsaturated and dry rocks. The resistivity of the saturated rocks in the upper part of the earth's crust, decreases with increasing their porosity and the degree of salinity of the saturated fluids. In contrary to the above, the presence of clay and conductive minerals can also reduce the resistivity of rocks which can be resolved by using other geophysical techniques, geological or well information. In resistivity surveying especially in vertical electrical sounding (VES), conduction in rocks is mainly due to pore fluids acting as electrolytes. Water in its pure form is poor conductor but most water contains dissolved salts which facilitate current flow. The resistivity of geological materials exhibits one of the largest ranges of all physical

properties from 1.6 x 10^{-8} Ω m for native silver to 10^{16} Ω m for pure sulphur (Reynolds, J.M., 1997).

The theory and basic principle of electrical resistivity method was described by different authors such as Telford *et al* 1990; Dobrin, M.B. and Savit,C.H.,1976; Parasnis, D.S.,1962; Robinson, C.S. and Caruh,C.,1988; Reynolds,J.M.,1997; Gibson, P.J. and George, D.M., 2003 so that only short descriptions of this method is included in this thesis.

2.2.2 Basic principle of electrical (dc) resistivity method.

The electrical conductivity of rocks can be studied by measuring the electrical potential distribution produced at the earth's surface due to an electric current which is injected in to the ground through electrodes for the cause of DC current. The types of currents introduced in to the ground are direct, commutated or low frequency alternative currents and the potential differences are measured using non-polarized electrodes.

The direct current sources are used to inject current in to the ground using two current electrodes to measure the generated electric field as a potential difference using other two potential electrodes.

If we consider the media that the current entered as a homogeneous isotropic ground, the flow of current in the medium is based on the principle of conservation of charge and is expressed by the relation

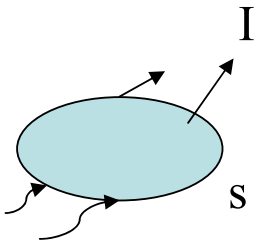

$$\left(I_c\right)_s = \frac{-dQ}{dt} \qquad (1)$$

where Ic is the current flowing out of the closed surface 'S' and 'Q' is the charge enclosed by 'S'. The current I_c and total charge Q can be expressed in terms of the current density **J** (the current I_c divided by the area over which the current is distributed) and the charge density **q** which is the total charge Q divided by the volume V as

$$\left(I_c\right)_s = \oint \vec{J}.d\vec{s} \quad \text{and} \quad Q = \int_v q dv \tag{2}$$

where V is the Volume bounded by the surface S.

Substituting the above equations into eq (1) and applying divergences theorem, we can get

$$\int_v \left(\vec{\nabla}.\vec{J}\right)dv = -\int_v \left(\frac{\partial q}{\partial t}\right)dv \quad \text{or}$$

$$\int_v \left(\vec{\nabla}.\vec{J} + \frac{\partial q}{\partial t}\right)dv = 0 \tag{3}$$

equation (3) is valid for any volume so that we can write it as

$$\vec{\nabla}.\vec{J} + \frac{\partial q}{\partial t} = 0 \tag{4}$$

equation (4) is called the law of conservation of charge in differential form and also known as the continuity equation.

For direct current, $\frac{\partial q}{\partial t} = 0$ so that eq (4) reduces to the form

$$\vec{\nabla}.\vec{J} = 0 \tag{5}$$

The electric field $\vec{E}$ is conservative field; it can be expressed as a gradient of the scalar potential function V as

$$\vec{E} = -\nabla V \tag{6}$$

where V is measured in volts.

From ohm's law; R = V/I, where V and I are the potential difference across the resistor with resistance R (Ω) and the current passing through it respectively. This expression can be written alternatively in terms of the electric field strength **E** (Volts/m) and the current density **J**(amp/m^2) as

$$\rho = \frac{E}{J}(\Omega m) \tag{7}$$

by taking only their magnitudes, the relation between the current density ($\vec{J}$) and electric field intensity ($\vec{E}$) can be given as

$$\vec{J} = \frac{1}{\rho}\vec{E} = -\frac{1}{\rho}\vec{\nabla}V \tag{8}$$

where ρ is a scalar function of the point of observation and $\vec{J}$ is in the same direction as $\vec{E}$ for isotropic medium.

From equations (5) and (8) we have

$$\vec{\nabla}\frac{1}{\rho}.\vec{\nabla}V + \frac{1}{\rho}\vec{\nabla}.\vec{\nabla}V = 0 \tag{9}$$

This equation is called the fundamental equation of electrical prospecting with direct current.

For homogenous medium, **ρ** is independent of the coordinate axes and equation (9) is simplified as

$$\vec{\nabla}.\vec{\nabla}V = 0 \quad \text{or} \quad \nabla^2 V = 0 \tag{10}$$

This is called the Laplace equation.

Therefore, the electrical potential distribution for direct current flow in a homogeneous isotopic medium satisfies the Laplace equation. The above equation has different forms in different coordinate systems. For example, using spherical coordinate system it can be expressed as

$$\frac{1}{r^2}\frac{\partial}{\partial r}\left(r^2\frac{\partial V}{\partial r}\right) + \frac{1}{r^2\sin\theta}\frac{\partial}{\partial\theta}\left(\sin\theta\frac{\partial V}{\partial\theta}\right) + \frac{1}{r^2\sin^2\theta}\frac{\partial^2 V}{\partial\phi^2} = 0 \tag{11}$$

Practically, the DC resistivity survey is conducted with two current electrodes (AB) called source and sink in which the current I (A) is injected in to the ground and two potential electrodes (MN) where the potential difference $\nabla V(V)$ is recorded.

If we consider (DC) source which delivers current I (A) to the homogenous, isotropic earth through the current electrodes, the potential at any point will vary as a function of r where r is the distance from the ground to the current electrodes. Figure 2.1 below shows the arrangement of current and potential electrodes, current lines and equipotential surfaces in a homogenous isotropic ground when the direct current source is used.

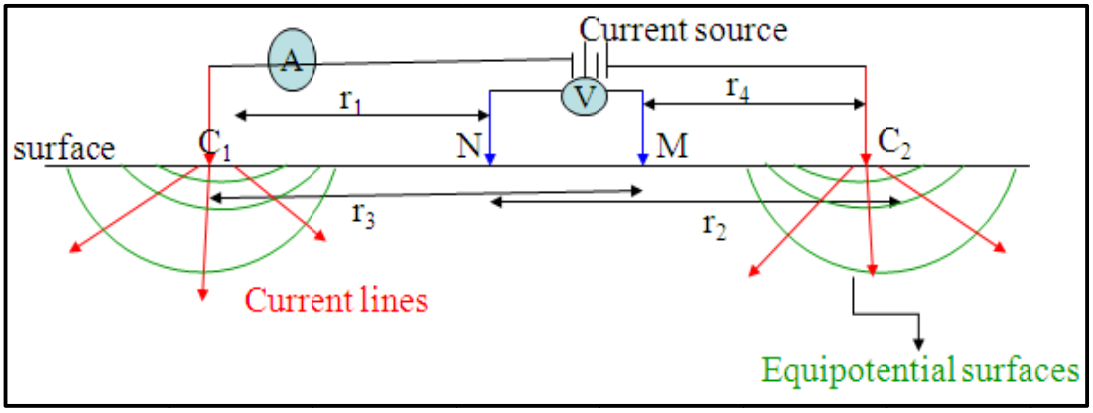

Figure 2.1 The arrangement of current and potential electrodes.

Assuming that the air above the ground has zero conductivity, the Laplace equation in spherical coordinate system is used to find the relation between the potential at r distance from the current electrodes so that equation(11) can be reduced to

$$\nabla^2 V = \frac{d^2V}{dr^2} + \frac{2dV}{rdr} = 0 \tag{12}$$

Since the potential varies only as a function r, $\frac{\partial V}{\partial \theta}$ and $\frac{\partial V}{\partial \phi}$ will be zero.

Multiplying equation (12) throughout by r^2 becomes

$$r^2 \frac{d^2V}{dr^2} + 2r\frac{dV}{dr} = 0 \tag{13}$$

Integrating both sides of this equation gives

$$V = \frac{-C_1}{r} + C_2 \tag{14}$$

where C_1 and C_2 are integration constants to be solved by using the following boundary conditions.

i. Since $V \to 0$ as $r \to \infty$ then $C_2 = 0$, **ii**, $\frac{dV}{dz} = 0$ at Z=0 and

iii, the current flows through a hemispherical surface in the lower half, so that $I = 2\pi r^2 J$ but $J = \delta E = -\delta \frac{dv}{dr}$ and $\frac{dv}{dr} = \frac{C_1}{r^2} \Rightarrow J = -\delta \frac{C_1}{r^2}$ so that $I = -2\pi\delta C_1$ or $C_1 = \frac{-I\rho}{2\pi}$ where ρ and δ are the resistivity of the ground and conductivity of the homogenous isotropic ground respectively. Therefore, equation (14) can be written as

$$V = \frac{I\rho}{2\pi}\left(\frac{1}{r}\right) \text{ or } \rho = 2\pi r\left(\frac{V}{I}\right) \tag{15}$$

When the distance between the two current electrodes is finite, the potential at any nearby point will be affected by both current electrodes. Therefore, the potential at N due to C_1 is

$V_1 = \frac{I\rho}{2\pi}\left(\frac{1}{r_1}\right)$ and due to C_2 at N is $V_2 = -\frac{I\rho}{2\pi}\left(\frac{1}{r_2}\right)$

because the current at the two electrodes are equal in magnitude but opposite in sign.

The total potential at N is given by

$$V_N = \frac{I\rho}{2\pi}\left(\frac{1}{r_1} - \frac{1}{r_2}\right) \tag{16}$$

Similarly the potential at M due to C_1 and C_2 is

$$V_M = \frac{I\rho}{2\pi}\left(\frac{1}{r_3} - \frac{1}{r_4}\right) \tag{17}$$

The potential difference measured between the two potential electrodes (MN) is

$$\Delta V = V_N - V_M = \frac{I\rho}{2\pi}\left(\frac{1}{r_1} - \frac{1}{r_2} - \frac{1}{r_3} + \frac{1}{r_4}\right) \tag{18}$$

where r_1, r_2, r_3, and r_4 are all in meters.

Therefore, after re-arranging the distances between the current and potential electrodes according to the well known configurations, we can determine the resistivity of the homogenous ground.

2.2.3 The Apparent Resistivity

If the ground is homogenous, the potential difference measured is as a function of the true resistivity of the homogenous earth and the geometrical factor. But in reality the ground is locally inhomogeneous and the potential difference measured depends on the current applied, the resistivity of the subsurface medium and the geometrical factor (k) determined by electrode array or configurations types. The resistivity calculated from such non homogeneous ground is not a true resistivity rather it is called apparent resistivity (ρ_a) which can be related to the parameters as

$$\rho_a = K\frac{\Delta V}{I} \tag{19}$$

This apparent resistivity has to be interpreted using curve matching or inversion techniques to find estimated resistivity versus depth of the subsurface.

There are many types of electrode configurations used in ground surveys, of which the most commonly used array are Wenner, Schlumberger, and dipole-dipole. Since the electrode separations relate to the investigation depth and the lateral resolution power required, one can choose the best electrode configuration for his planed survey at the initial of his survey. The expression for apparent resistivity in each of the above array types will be different due to the difference in the geometrical factor (k) of each array types.

Let us take the Schlumberger array in which the electrodes are symmetrically placed a point at the center of the array as shown below in Figure 2.2.

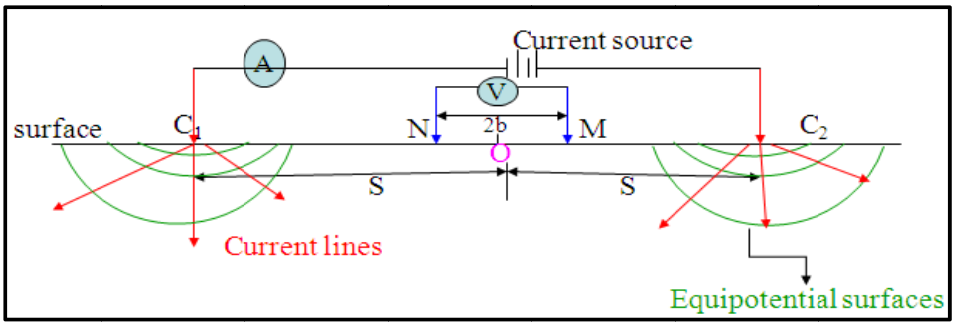

Figure 2.2 The electrode arrangement of schlumberger array.

Where r_1=s-b,r_2=s+b,r_3=s+b and r_4=s-b and O is the center of the array.

The potential difference ΔV using eq(18) is given by

$$\Delta V = \frac{I\rho}{2\pi}\left(\frac{2b}{s^2 - b^2}\right) \tag{20}$$

and $$\rho_a = \pi\left(\frac{s^2 - b^2}{2b}\right)\left(\frac{\Delta V}{I}\right) \tag{21}$$

where the geometrical factor $K = \pi\left(\frac{s^2 - b^2}{2b}\right)$ and it is different for different arrays.

In addition to the array types, one will choose the appropriate resistivity survey procedures depending on the objective of the study. Some of the most commonly used procedures in resistivity surveying work are resistivity profiling, resistivity soundings and electrical surface imaging. Depending on the specific objectives and the geology of the area, one can use profiling mainly to obtain information on lateral variations in resistivity, resistivity sounding to determine the variation in resistivity in the vertical direction of horizontally stratified layer earth or electrical surface imaging which combines surface profiling with vertical soundings using a multi-electrode array to produce two dimensional (2D) or three dimensional (3D) images of the subsurface.

2.2.4 Vertical Electrical Sounding (VES)

Vertical electrical sounding (VES) consists of a symmetrical electrode array used to determine the resistivity of the subsurface which is assumed to be horizontally stratified layers. The procedure is used to determine the variations in resistivity in the vertical direction and called electrical drilling or commonly vertical electrical sounding (VES). By expanding symmetrically the distance between current electrodes about a point called the sounding point, while keeping the potential electrodes MN at the same position, provides a sounding curve corresponding to the apparent resistivity versus depth of the location. As the spacing between the current electrode increases, the investigated depth will also increase.

The two most commonly used arrays in electrical sounding survey are the Wenner and Schlumberger arrays. In this work, we have used the data which was collected by using the Schlumberger electrode array techniques. When the Schlumberger array is used, the distance between the potential electrodes is not greater than one tenth of the current electrodes spacing. The advantage of this array is that initially only the spacing between the current electrodes is increased. However, at large current electrode spacing, the measured potential becomes very low and the distance between the potential electrodes is increased. Increasing the potential electrode spacing produces a 'step' in the apparent resistivity curve and it is good practice to obtain an overlap between the curve segments by obtaining two readings at different potential electrode spacing for two adjacent current electrode spacing. Segments obtained at larger potential electrode spacing can be shifted in order to produce a smooth curve (Gibson, P.J. and George, D.M., 2003).

2.3 Theory of Gravity Method

2.3.1 General

Gravity is one of the four fundamental forces of nature which controls all moments of mass on earth. In exploration geophysics, gravity surveying is conducted to investigate the subsurface geology based on variations in the earth's gravitational field caused by difference in density between rocks beneath the earth's surface. The gravitational attraction of a body of non-homogenous density will vary from one measuring point to another due to difference in the distribution of density in the body. These variations in gravitational attraction of the earth from point to point will provide valuable information about the subsurface geology. Gravity surviving uses gravity meters to measure these lateral variations in density. The final interpreted data will give a good structural trend of the subsurface rocks based on difference in density. Rock densities that give rise to gravity anomalies are among the least variable of all geophysical parameters. The density of a rock depends on both its composition and porosity. Most common rock types have densities in the range between 1.6 and 3.2 g/cm^3.

The theory and basic principle of gravity method was described by different authors such as Telford *et al* 1990; Dobrin,1976; Parasnis,1962; Robinson *et al* 1988; Reynolds,1997; Gibson,

P.J. and George, D.M.,2003; and Blakely, J.R., 1996 so that only short descriptions of this method is included in this thesis.

2.3.2 Fundamental Principles of Gravity

The bases for the gravity method are the two laws of Sir Isaac Newton. These are;
Universal law of gravitation:

$$\vec{F} = -\frac{GM_E m}{r^2}\hat{e}_r \tag{22}$$

and second law of motion:

$$\vec{F} = m\vec{g} \tag{23}$$

We can combine them to obtain the gravitational acceleration at the surface of the earth, which is given as

$$\vec{g} = -\frac{GM_E}{R_E^{\,2}}\hat{e}_r \tag{24}$$

where $\vec{F}$ is the force of attraction, R_E is the earth's radius from its center, M_E is the mass of earth, m is the mass of an object and r is the distance between the two masses, $\hat{e}_r$ is the unit vector directed away from M_E towards m, and G is the universal gravitational constant with value of $6.67259\text{x}10^{-11}\text{m}^3\text{Kg}^{-1}\text{S}^{-2}$ in SI unit or $6.67259\text{x}10^{-8}\text{m}^3\text{g}^{-1}\text{S}^{-2}$.

The gravitational acceleration also called the gravity filed intensity of the Earth $\vec{g}$ various radially from the earth's center and has an average value of -980 cm/s^2, a value at about 45^0 latitude on the surface. The measured value of the gravitational acceleration around Addis Ababa is about -977.5 cm/s^2. The negative sign shows the force is attractive.

2.3.3 Gravitational Potential

Gravitational fields are conservative since the total energy of an object in this field depends only on its position rather than the path it follows. These conservative fields can be expressed by a scalar function called gravitational potential U(r) which varies with distance or position relative to the mass only.

The gravitational potential U(r), due to a point mass m_1 at a distance r from m_1, is the work done by the gravitational force in moving a unit mass from infinity to a position r from m_1 along any path. Mathematically it is given by

$$U(r) = \int_{\infty}^{r} \vec{g}\, d\vec{r} = -Gm_1 \int_{\infty}^{r} \frac{dr}{r^2} = \frac{Gm_1}{r} \tag{25}$$

where $\vec{g} = -\frac{Gm_1}{r^2}\hat{e}_r$. Alternatively, we can get $\vec{g}$ by finding the gradient of the potential function U(r) as

$$\nabla U(r) = -\frac{\vec{F}(r)}{m_2} = -\vec{g}(r) \tag{26}$$

U is a scalar field which makes it easier to determine $\vec{g}$ from it as shown above and we can also express $\vec{g}$ in terms of a scalar potential function U(r) which is the case that we call it a potential field technique in exploration geophysics. The quantity which is measured by gravimeters in gravity surveying is the only vertical component of $\vec{g}$ which can be found from the scalar potential function U(r) as

$$g_z = -\frac{\partial U}{\partial z} \tag{27}$$

The c.g.s unit for acceleration due to gravity is cm/s^2 which called Gal named in honor of Galileo. The other subunits used by geophysicists to measure acceleration due to gravity include milligal (mgal), micro gal (μ gal) and gravity unit (g.u.). In the SI unit system, it is measured

by m/s^2 but it is rarely used in field measurements because the mgal and in some cases the μ gal units are commonly used in gravity measurements than the other units.

2.3.4 Earth's Shape and its Gravity Field

Geodesists use different meanings for the expression 'Figure of the earth' according to the way it is used and the precision with which the earth's size and shape is to be defined. Different disciplines use different surfaces as a representation of earth. Topographers and hydrographers use the actual topographic surface whereas many astronomical and navigational computations use a spherical earth model due to simplicity in mathematical computation. Even if a sphere is close approximation to the true figure of the earth and is satisfactory for many purposes, geodesists who use measurements of long distances along continents and oceans represent the earth as an oblate spheroid or oblate ellipsoid from results of modeling the shape of the entire earth. The oblate ellipsoid used in geodesy to most nearly approximate the earth's shape is flattened at the poles and bulged at the equator and is obtained by rotating an ellipse about its minor axis.

In contrary to the above, if we consider the shape of earth as a sphere, the field of gravitational attraction of the earth on a small object of mass m which moves with a velocity V on the surface of the earth that rotates with angular velocity ω will be the resultant of the forces ; gravitational attraction due to the earth's mass ($\mathbf{F}_m$), the tidal force due to mass attraction of other heavenly bodies(**T**) , centrifugal forces(F_ω) and Coriolis forces(F_c) due to the rotation of the earth with ω and its linear velocity V on the earth's surface respectively.
Mathematically the net acceleration on m is given by;

$$\vec{g} = \vec{g}_m + \vec{g}_\omega + \vec{g}_c + \vec{T} \tag{28}$$

where $\vec{g}_m = \frac{GM}{R^2}$,R is the radius of spherical earth, $\vec{g}_\omega = \vec{\omega} \times (\vec{\omega} \times \vec{R})$ and

$\vec{g}_c = 2(\vec{\omega} \times \vec{R})$ .If the mass m is at rest (V=0) on the surface of the earth which is the case for

most measurements, then the value of $\vec{g}_c$ will be zero. In actual works, the value of $\vec{T}$ will be reduced after data collection using different softwares. So that the gravitational attraction on m after $\vec{T}$ was corrected will be the combined effects due to the earth's mass acceleration and rotational (centrifugal) acceleration which is given by;

$$\vec{g} = \vec{g}_m + \vec{g}_\omega \quad \text{or} \quad \vec{g} = \frac{GM}{R^2}\hat{e}_r + \vec{\omega} \times (\vec{\omega} \times \vec{R}) \tag{29}$$

Therefore, the Earth's gravity potential (W) on the surface of the earth is the sum of the mass gravitational potential (U_m) and the centrifugal potential (V_ϕ).

$$W = U_m + V_\phi \quad \text{and} \quad \vec{g} = gradW \tag{30}$$

2.3.5 The Reference Ellipsoid, Geoid and Plumb Lines

The shape of the earth, determined by the geodetic measurements and satellite tracking is nearly spheroid, bulged at equator and flattened at the poles. The polar flattening of this ellipsoidal earth is $(R_{eq}-R_p)/R_{eq}=1/298.257$, where R_{eq} and R_p are the earth's equatorial and polar radii respectively. The international reference ellipsoid is a mathematical surface which is used to describe the figure of the earth and is a close approximation to the equipotential surface of gravity.

The surfaces of constant gravity potential (W=const) are called equipotential surfaces or level surfaces. The surface of quit oceans are the part of this level surface called geoid. After C .F. Gauss, the geoid is considered as the mathematical surface of the Earth as opposed to the visible topographical surface. The Geoid represents a surface over which the gravitational field has equal value and is called an equipotential surface. The irregular distribution of mass, especially near the ellipse of rotation, warps the geoid so that it is not identical to the ellipse of rotation.

Figure 2.4 below shows the plum lines intersect the level surfaces orthogonally they are not quit straight rather very slightly curved. The direction of gravity vector defines the vertical or plumb lines.

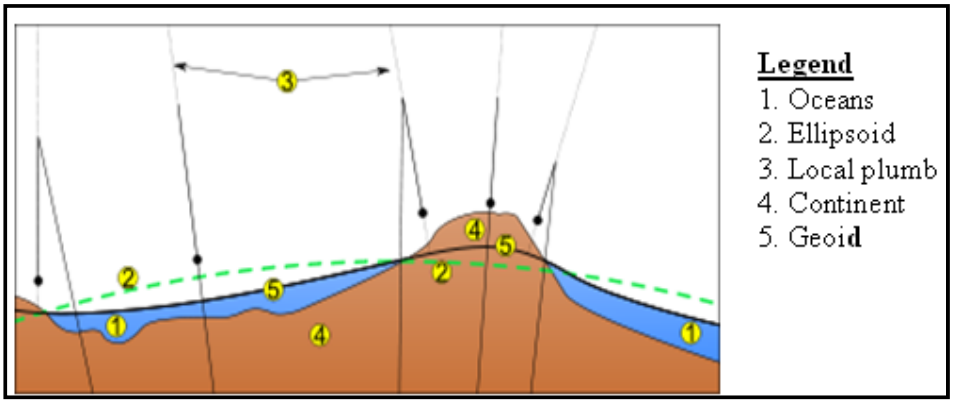

Figure 2.3 The relationship between reference ellipsoid, geoid, local plumb at oceans and continents (Wikipedia, 2011).

2.3.6 Theoretical (Normal) Gravity

The theoretical or normal gravity value γ_N on the rotating reference ellipsoid can be computed by differentiating the gravity potential (W) shown in eq (30)

$$\gamma_N = gradW \tag{31}$$

where (W) is the ellipsoidal Earth gravitational potential which includes the mass gravitational potential (U_m) and the centrifugal potential (V_ϕ) as described above in eq (30).

The variation of the theoretical gravity value (γ_N) which is normal to the ellipsoidal surface can be derived by making the required mathematical treatments on the eq (31) and it can be written as

$$\gamma_N = \gamma_e\left(1 + \beta \sin^2\phi - \beta_1 \sin^2 2\phi\right) \tag{32}$$

Where γ_e is the value of gravity at the equator $\phi = 0$, β and β_1 are constants determined from the gravity flattening. Equation (32) is known as the normal gravity formula or the geodetic reference formula. The formula used to find the normal or theoretical gravity value at any latitude ϕ on a rotating ellipsoid (eq 32) was revised in 1967 by the International Union of geophysics and Geodesy and adopted a revised normal gravity formula given by

$$\gamma_N = 978031.846\left(1 + \beta \sin^2 \phi + \beta_1 \sin^4 \phi\right) mgal \tag{33}$$

where γ_e =978031.846mgal, β =0.005278895 and β_1 =0.000023462.

The above equation is called the 1967 geodetic reference system (GRS-67) (Reynolds, J.M., 1997).

The theoretical or normal gravity formula used for this thesis to reduce the gravity data is called the 1980 geodetic reference system (GRS-80) (Moritz. H., 2000) and it is given by

$$\gamma_N = \gamma_e \frac{1 + K \sin^2 \phi}{\left(1 - e^2 \sin^2 \phi\right)^{1/2}} \tag{34}$$

where γ_e=978032.67715mgal, $k = \frac{b\gamma_p}{a\gamma_e}$ -1=0.001931851353, and $e^2 = \frac{a^2 - b^2}{a^2}$

=0.00669438002290 is called the first excentricity, a =6378137m and b = 6356752.3141m are called semi-major and semi-minor axis respectively.

Using the series expansion for the eq (34) with the appropriate constants, it becomes

$$\gamma_N = \gamma_e \begin{pmatrix} 1 + 0.0052790414 \sin^2 \phi + 0.0000232718 \sin^4 \phi \\ + 0.0000001262 \sin^6 \phi + 0.0000000007 \sin^8 \phi \end{pmatrix} \tag{35}$$

The world geodetic system (WGS) coordinate system is also geocentered coordinate frame which was used as a standard spheroid reference surface. This coordinate system which includes the earlier schemes as WGS60, WGS66, WGS72 and the recent WGS 84 is used as a reference coordinate system for Global Positioning Systems. For this work, the GRS-80 (Moritz.H., 2000) ellipsoidal reference system was used for gravity data reductions and WGS-84 was used for the DGPS data processing. The minute difference between GRS-80 and WGS-84 results from refinements to the latter's defining constants and has no effect for all practical purposes (Li, X. and G¨otze, H., 2001).

2.3.7 Gravity Base Stations

Relative gravimeters are mostly used in regional or local gravity surveys and measure the relative gravity value Δg between the observation sites. Therefore, in order to relate the gravity value of each observation sites with the global network, at least one easily accessible gravity base station with absolute gravity value must be available. One of such gravity network is the International Gravity standardization Net 1971(IGSN71).

The absolute value at each observation site is determined by tying with the global reference, the International gravity Standardization net (IGSN71). Hence, the absolute gravity value (g) at the observation sites can be found as;

$$g = g_r + \Delta g \tag{36}$$

Where, g_r is the absolute gravity at the base station and Δg is the gravity difference between the base station and observation site after tide and drift corrections have been done (Robinson ,S.C. and Caruh, C., 1988).

2.3.8 Corrections to Gravity Observations

Most relative gravimeters do not give direct measurements of gravity, rather a dial reading is taken to be multiplied by an instrumental calibration factor to produce a value of observed gravity (g_{obs}). However, there are some modern gravimeters that use Feedback System to directly measure the gravitational acceleration difference between two stations. These observed gravity values are different from place to place due to Instrumental drift, Earth tides, local topography or terrain, latitude, height and surface density variations. Before the results of the survey are interpreted in geological terms, the raw gravity data have to be corrected to a common datum, such as to the ellipsoid surface, in order to remove the effects of features that are only of indirect geological interest .The difference between the values of observed gravity(g_{obs}) and determined either from the international gravity formula/geodetic Reference system 67 or 80 for the same location ,or relative to local base station, is known as the gravity anomaly.

The various corrections that can be applied are classified mainly as temporal and spatial variations.

2.3.8.1 Temporal Based Variations

The main factors that can cause time dependant variations in the gravity measurements include instrumental drift, tare and tidal effects, temperature and pressure effects. While the first two are related with the instrument character and how it is handled, the last three are external factors that vary not only temporally but spatially also.

A) Tide Corrections.

If we make continuous gravity measurement at a station, the gravity value will change at each sampling time mainly due to tidal effect, which is caused by the relative attraction of the moon, the sun and other celestial bodies which should be corrected before any other corrections. The fluctuation of gravity value δg_T can be calculated using a equations based on the masses of the moon and sun and their positions relative to an observation site, but these formulae are long and complicated so that computer programs are used to make the calculations. Moreover, site specific correction can be made using models that are based on observation for that particular area. The other alternative is to use repeated measurements (1-2 hours) at measurement points and remove the tidal effect together with the instrument drift.

B) Drift and Tare Corrections.

Gravimeter readings change with time as a result of elastic creep in the springs, producing an apparent change in gravity at a given station. The instrumental drift can be determined simply by repeating measurements at the same stations at different times of the day, typically 1-2 hours. The difference between successive measurements at the same station are plotted to produce a drift curve. Observed gravity values from intervening stations can be corrected by subtracting the amount of drift from the observed gravity value (Reynolds, J.M., 1997). Another alternative approach is to use the adjustment of the repeated measurements using the least-square approach or the robust estimation techniques.

If the instrument faced excessive jerk between readings or subjected to sudden motion or jarring as during transport, somewhat erratic changes called tares may be occurred. If the instrument is

bumped, it is wise to reread a known station immediately. There is no way of allowing for erratic changes, we can only correct those points occupied while the drift curve is smooth (Telford *et al* 1990).

2.3.8.2. Spatial Based Variations.

These are changes in the observed gravitational acceleration which are space dependant. These variations change the gravitational acceleration from places to place but these are not related to the subsurface geology which need to be corrected.

A) **Free air correction**

Though gravity value at any place varies inversely with the square of distance, it is necessary to correct for changes in height between stations to reduce field readings to a datum surface (reference ellipsoid). The free air correction doesn't take account of the material between the station and the datum plane (Telford *et at* 1990).
Assuming the earth to be sphere rather than an oblate spheroid and its mass concentrated at its centre of mass, the value of gravity at sea level is give by

$$g_0 = \frac{GM}{R^2} \tag{37}$$

The value of gravity at station located at a height of h meters above sea level is;

$$g_h = \frac{GM}{(R + h)^2} = \frac{GM}{R^2}\left(\frac{1 - 2h}{R} \ldots\right) \tag{38}$$

The difference in gravity between sea level and at h meters is the free-air correction

$$\delta_{gF} = g_0 - g_g = \frac{2g_0 h}{R} \tag{39}$$

With $g_0 = 981.7855$ gal, R=6371000 meter and h is in meter.

$$\delta_{gF} = 0.3082 hmgal \tag{40}$$

But the earth's shape is an oblate spheroid rather than a sphere so that the normal accepted value of the free air correction is

$$\delta_{gF} = \frac{0.3086h(mgal)}{metre} \tag{41}$$

This free-air correction value will be added to the measured gravity value at stations located above the reference ellipsoid and subtracted when observation points are below it.

B) Latitude Corrections.

The shape of the Earth, determined by geodetic measurements and satellite tracking is nearly spheroid, plugging at equator and flattened at the poles.

Both the rotation of the Earth and its equatorial bulge produce an increase of gravity with latitude. This latitude correction is usually made either by using the relation

$$0.000811\sin 2\phi \frac{mgal}{m} \tag{42}$$

or it will not be necessary if the normal gravity value is removed from the measurement.

C) Bouguer Correction.

The Bouguer correction accounts for the attraction of material between the point of measurement and the reference ellipsoid which was neglected in the free-air correction. Using the assumptions that the space between the measurement point and the reference ellipsoid is filled by a slab having uniform density and infinite horizontal extent, one can calculate the effect of this infinite slab of thickness h and density δ on the measuring point by using the formula

$$\delta g_B = G\sigma 2\pi h \tag{43}$$

If we take G=6.67259x10^{-8} $cm^3g^{-1}sec^{-2}$ and σ is in gm/cm^3 and h in meter, the Bouguer correction (δ_{gB}) is given as

$$\delta_{gB} = 0.041925\sigma h(mgal) \tag{44}$$

The effect of this intermediate layer or slab is called the Bouguer effect and the correction taken is called the Bouguer correction which has the opposite sense to the free-air correction. This means that the correction value will be subtracted when the station is above the reference ellipsoid and added when it is below the reference ellipsoid.

D) Terrain and Isostatic Corrections.

The Bouguer correction practice assumes only the mass between the reference ellipsoid and measuring point to be an infinite slab is not appropriate when there is a topographic change in the survey area. This is because of that what one may face actually is not only the infinite slab but also hills, gorges, rivers etc around the measuring point. Hills above the height of the gravity observation station exerts an upward pull on the gravimeter, whereas valleys below it fail to pull down ward on it which was filled by infinite slab during the Bouguer correction that increases the gravity reading but didn't exists in reality. The terrain correction accounts for such types of surface irregularities in the vicinity of observation stations. There are several ways to calculate the topographic effects, among these, the two most commonly used ways are the chart method before the advent of computers and the prism method after the advent of computers.

The aim of the Isostatic correction is to remove the effects on g_{obs} caused by the large scale change in density due to lateral variations in the density of the upper crust. The average Bouguer anomaly in oceanic areas is generally positive, while over mountainous regions, it is usually negative. These effects indicate that the rocks found beneath the oceans are denser whereas the rocks found beneath mountains are less dens than normal. Two hypotheses were proved in the 1850s to account for this large-scale systematic variation in density. The geodesist G.B.Airy (1855) proposed that while mountain chains had deep roots beneath the oceans, the crust which was assumed to have constant density everywhere is thin. In contrast, an English Archdeacon J.H.Pratt (1859) thought that the crust extends to a uniform depth below sea level but that density varied inversely with height of the topography (Reynolds, J.M., 1997).
The study area has no such rugged topography to conduct the terrain correction and it is not large area to perform Isostatic correction. Therefore, neither of the two corrections was done to the gravity data used for this work.

2.3.9 Gravity Anomalies

Any change in gravity reading at the observation point, after all the previous corrections have been done, is associated to variations on density of the subsurface geological structures at locally or irregularity in the thickness of the earth's crust globally. These effects are indicated by patterns of gravity anomaly variations over the survey area. The major types of gravity anomalies which are used to study the subsurface geology on the earth's gravitational field are the free air anomaly, the simple Bouguer anomaly and the complete Bouguer anomaly.

A) The Free-Air Anomaly (Δg_{FA})

The free-air gravity anomaly at each observation site is calculated by

$$\Delta g_{FA} = \left(g_{Obs} \pm 0.3086h - \gamma_N\right) mgal \tag{45}$$

Where g_{obs} the observed gravity in mgal, h is the height from the reference ellipsoid to the observation point in meter, r_N is the normal gravity on the reference ellipsoid at that latitude in mgal and Δg_{FA} is the free air anomaly in mgal.

Since Δg_{FA} is corrected for height, latitude dependant, and earth's rotation and flattening effects change in its value is correlated with the local topography.

The free-air anomaly (Δg_{FA}) will have positive value for observation points located above the reference ellipsoid and negative value for those observation points located below it.

B) The Simple Bouguer Anomaly (Δg_{SBA})

The simple Bouguer gravity anomaly which accounts for the effect of the mass of the intermediate layer between the reference ellipsoid and observation points is given by

$$\Delta g_{SBA} = \left(g_{Obs} \pm 0.3086h - 0.041925\sigma h - \gamma_N\right) mgal \tag{46}$$

Its difference from the free-air anomaly is that it considers the effect of the intermediate layer but it doesn't account for the topographic correction.

CHAPTER THREE

DATA ACQUISITION AND PROCESSING

3.1 General

The Oromia water works design and supervision enterprises selects some areas in Borena zone to be studied in detail for groundwater exploration based on the previous detailed geological and reconnaissance geophysical surveys. These areas are planned to be studied in detailed by using different geophysical techniques. Gelchet is among those areas selected for detailed study to understand the different lithologic units, ground water potential zones, geological structures and the physical properties of subsurface rocks using integrated geophysical techniques.

3.2 The Geoelectric Data

The Electrical resistivity method is used to study the resistivity of the subsurface rocks. The vertical (1D) electrical sounding survey was used in this study to identify the water-bearing horizons, the number of layers, their thickness and resistivities.

3.2.1 Instrumentation

The geoelectric data were acquired using IRIS Instrument SYSCAL R1 PLUS Switch-72 which is a new all-in-one multiple resistivity imaging system. It features an internal switching board for 72 electrodes and an internal 200 W power source. It is compact, easy to use and field proof. The SYSCAL R1 PLUS Switch-72 measures both resistivity and chargeability (IP).

3.2.2 Resistivity Data Acquisition

The resistivity survey was conducted along eight survey lines oriented approximately east- west and north-south with in the area. The spacing of VES points were not uniform due to accessibility and expected geological structures. The VES survey was started with 1km from each of north, south, east and west margins and conducted with VES separation ranging from 2 to 3km.

Total of twenty eight vertical electrical sounding points (VES) along eight different survey lines, using Schlumberger configuration with AB/2 spacing ranging from 1.5m to 1000m, were surveyed in the study area. Some of these VES were surveyed near to the previously drilled boreholes. The apparent resistivity, voltage and current for different electrode spacing and the location of VES points were recorded. Figure 3.1 shows the location of VES points and drilled boreholes.

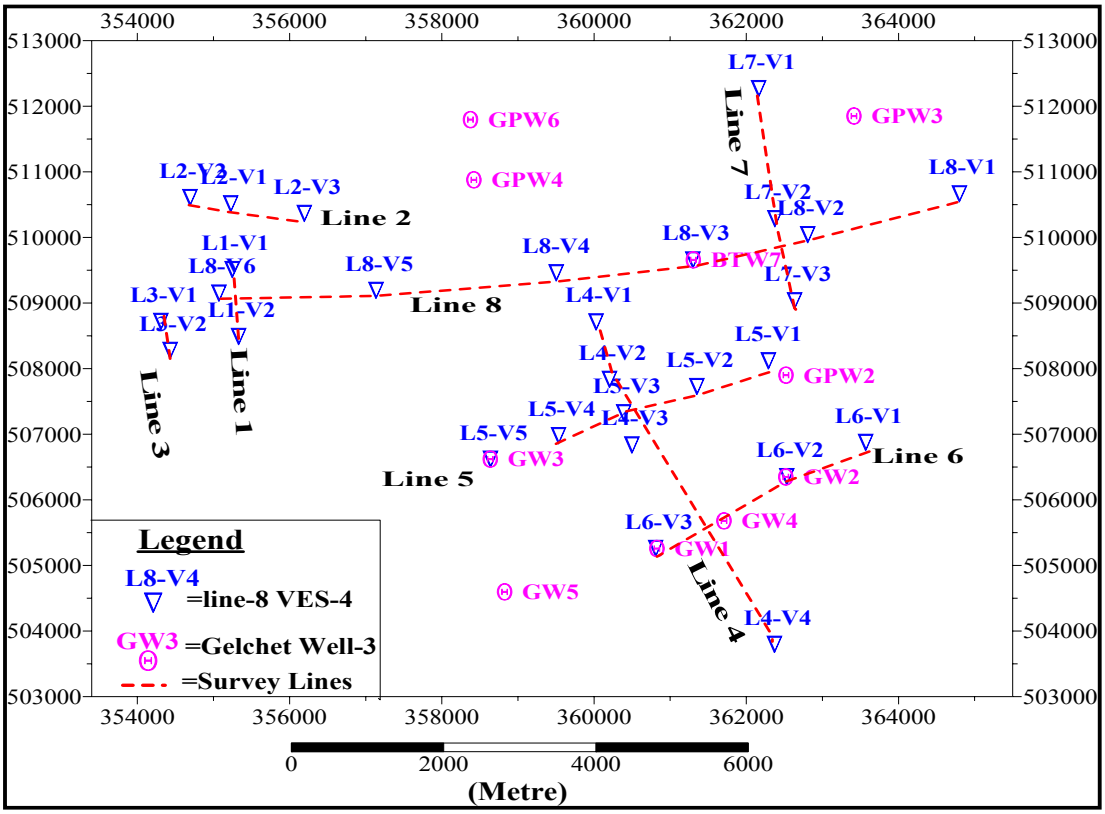

Figure 3.1 Location of the vertical electrical sounding (VES) points and Boreholes.

3.2.3 Electrical Data Processing

After the field data have been collected, the raw resistivity data were entered to the excel sheet and prepared for other software. The apparent resistivity pseudodepth section along profiles and the apparent resistivity sliced pseudodepth map of the whole area for different current electrode spacing were prepared by using surfer8 software. The one dimensional (1D) molding of VES data was done by using resistivity modeling software called Resix-IP and WinResist. The depth and resistivity of subsurface rocks beneath VES points were determined from the one

dimensional inversion of VES data. The parameters from the modeled VES (resistivity and depth) are used to make the geoelectric sections along two survey lines (Line-6 & 8) by using AutoCAD drawing software and later modified by Sulfer8 software.

3.2.4 Ambiguities of Sounding Curve Interpretation.

The Vertical electrical sounding curve modeling and interpretation is inextricably linked with the principle of equivalence. The principle expresses that a measured sounding curve is basically related with many physically equivalent models that may differ considerably. The VES data can be interpreted with different number of layers without any preference. Another important property of vertical electrical sounding curves is evident. By all appearances, only the minimum number of layers can be deduced implying that thin layers are preferentially suppressed. A rule of thumb indicates that a layer becomes clearly visible in a sounding curve if its thickness is comparable to its depth of deposition (Kirsch, R., 2006). To avoid the ambiguity of equivalence in the 1D inversion of VES data and check the continuity of layers in the area, the data of three boreholes (GW1, GW2 and BTW7) were used to fix model parameters and tried to get depths independent of equivalence for L8-V3, L6-V3 and L6-V2. Once the resistivity and depth for the above mentioned VES were determined by fixing their depth from the boreholes (lithology data) using Resix-IP software, the depth and resistivity of the other VES along these survey lines were estimated by using the principle of parameterization.

The resistivity parameters which were estimated form constrained and parameterized 1D inversion of VES data using Resix-IP software, were used as initial model for WinResist software to find the final resistivity layer parameters. The software WinResist uses iterations techniques to adjust the fitting between the observed data curve and the initial model parameters. Several reinterpretations for modeled soundings curves were performed to get better model parameters and the iteration process was finalized when the root mean square (RMS) errors was less than 5%.

3.3 The Gravity Data

The significance of gravity data with respect to a hydrogeological situation depends mainly on the accuracy achieved in the field survey. Basic requirements for an accurate data set are

gravimeters with well known physical characteristics, a well designed survey, high precision measurements, and state of the art data processing (Kirsch, R., 2006).

In the study area, the gravity survey was conducted with the assistance from DGPS survey. The DGPS survey is used to precisely locate each gravity station, which is essentially needed in the gravity reductions.

3.3.1 Pre-Measurement

The determination of the crude location of gravity station is used to approximate the theoretical gravity anomaly variation which is essential to design the survey plan such as daily measurement plan and to choose the appropriate range of the gravimeter reading. Moreover, the pre-survey preparations included the determination of the sampling interval, location of data points on appropriate scale maps, tidal table compilation, calibration of instrument and the determination of the theoretical gravity values using the available height information.

The gravity station separation and survey lines were chosen based on the available geological information (OWWDSE, 2008)), previous geophysical survey outputs (such as VES) and accessibility. Based on the above information, a measurement interval of 300 to 500m was chosen, which was sometimes modified in the field when the need arise to 800 or 1000m interval.

3.3.2 Instrumentation

The upgraded Lacoste and Romberg(L&R) stable type gravimeter with a model number of G781, which measures relative gravity values between gravity station was used in the gravity survey. The gravimeter uses a feedback system and is thermostatically controlled with an internal temperature of 51.9^0C. It uses a 12 volt Nickel-Cadmium battery source always connected with it to prevent variation in gravity reading caused by internal temperature fluctuation. The new Aliod 100 feedback system has a range of approximately 100mGal (+/-50) with a resolution of 0.001mGal (Lacoste and Romberg, 2003) at a particular dial reading and displays the measurements digitally in milligal (mgal) value. These futures of the gravimeter make it flexible to be used in detailed or regional surveys.

The instruments used for GPS survey were Trimble R_7 receiver, Trimble Zephyr geodetic antenna, a fixed height bipod antenna with a spike mount system, 12V battery as a power supply, a solar panel connected to the battery to recharge it and at the same time serve as a power source whenever there is enough solar radiation, water level, compass and a hand held GPS receiver to roughly locate predetermined measurement positions.

3.3.3 Gravity Data Acquisition

Before the field campaign, the gravimeter was calibrated using standard calibration techniques and its performance was tested at known sites. Depending on the theoretical gravity value of the study area, the range of the instrument was set to accommodate the expected gravity value in the area. Then the dial reading was set to a fixed position of 1282.4 to let the feedback system take over the automatic balancing of the measurement beam. The value of a station very near to the field camp but far away from the measurement area was taken as a reference value for there are no stations with an absolute gravity value for referencing. This base station is marked with a stainless still bolt, so that in the future it will be connected with known absolute gravity stations.

Whenever possible the transportation between measurement points was carried out using 4-wheel drive vehicles and when not the gravimeter was carried on the back of individuals, sometimes for a whole day. Since the area is covered by dense thorny bushes, which made the travel between measurement points very difficult, a combination of leapfrog method and closing at base stations were used to collect the gravity data.

The first step was always to roughly locate the predetermined station location using a hand held GPS receiver. Then depending on the availability, either the gravity or GPS measurement was taken first. During gravimetric reading the station number, location, date, time, dial reading, Mgal values, instrument height, air-pressure and temperature were always recorded.

A total of one hundred and fifteen gravity stations have been used to cover the study area. Out of these measurement points at 68 station repeated measurements were taken, which is 59 % of the total number of stations. The distance between neighboring gravity stations ranges between 300 to 500 meters along profiles, and 800 to 1000m for some infill stations between the survey lines.

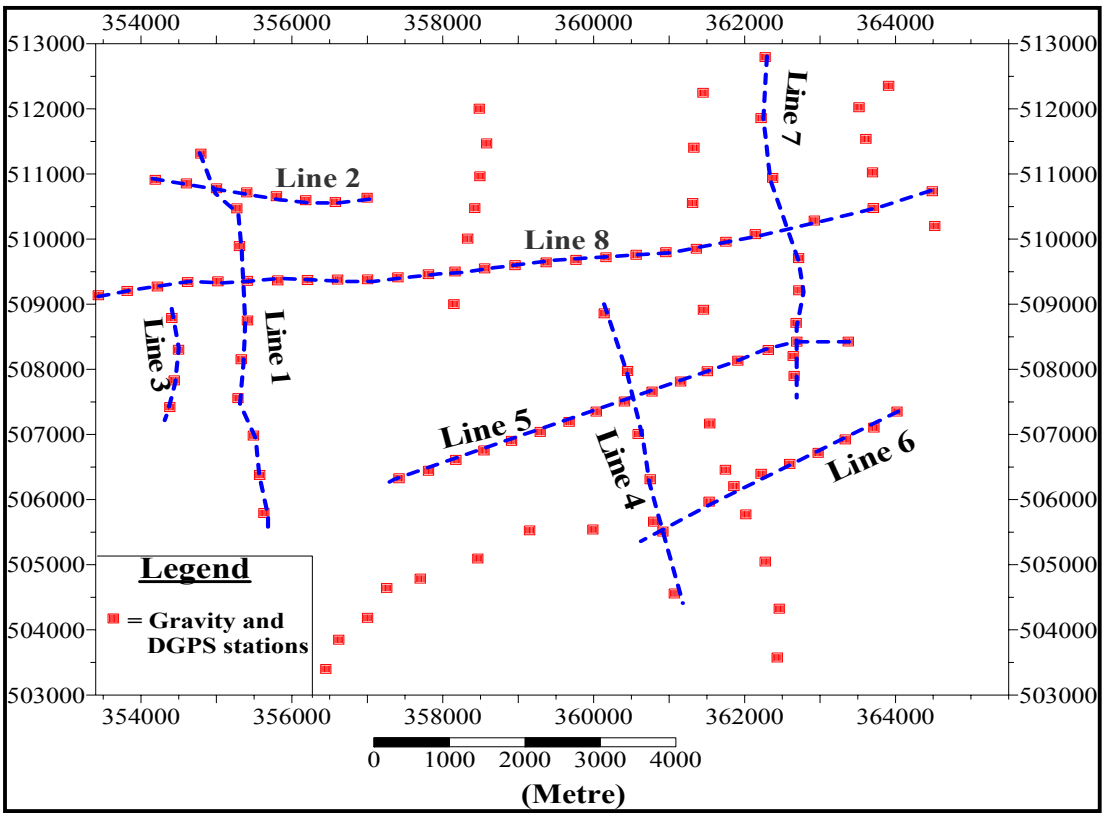

Figure 3.2 Location of gravity and GPS stations.

3.3.4 Gravity Data Processing

The Global positioning system (GPS) data were processed before the gravity data to get accurate coordinates for each gravity stations. The GPS data collected in a fast static mode for the whole survey area were first downloaded from the GPS receiver and processed using the Trimble Geomantic office (TGO) software. This software processes the "RINEX" and "DAT" files of the GPS data. Before the field data were processed, the GPS data from the reference station at Arba-Minch University (155 km air distance from the survey area) run by the Institute of Geophysics, Space Science and Astronomy of Addis Ababa University in collaboration with the University of Montana, and Massachusetts Institute of Technology as well as UNAVCO from USA for the same time interval were downloaded for referencing. The coordinate of Arba-Minch permanent GPS station X=6.06242766^0 Y=37.56085206^0 and Z=1199.8885m above WGS 84 ellipsoidal reference system was known in the International terrestrial reference frame (ITRF)2005 system with an accuracy of $\delta_X = 0.00159, \delta_Y = 0.00135$ and $\delta_Z = 0.00043$meters

(Abebe, E., 2010). During the processing of the filed data, the coordinates of the permanent station were used as a reference value .The minimum error of position measurement found after processing the GPS data was $\delta_X = 0.00345$, $\delta_Y = 0.00287$ and $\delta_Z = 0.00534$ meters while at some points the error was as large as $\delta_X = 0.0122$, $\delta_Y = 0.0091$ and $\delta_Z = 0.0213$ meters.

The gravity data recorded on the gravity data log sheet in the field were entered to excel to prepare it for reduction. Using the software SM4PC (Becker, M., 1984), the gravity data were first corrected for tidal and pressure effects. Then the instrument height was removed and data points were reduced to the ground surface. Using the program GRAUS (Becker, M., 1984) the repeated gravity measurements were adjusted and drift values were corrected to get a drift free single measurement at a station. As a result, the mean square error in the area was found to be 10.6 μgal which make the survey a high precision survey.

The raw gravity data (corrected for temporal variations) were then corrected for spatial variations such as atmospheric effects, Free-air and intermediate layer reductions using the software GRAVRED (Lewi, E., 1997) to yield the Free-air and Bouguer anomalies respectively. The coordinates of each gravity stations were taken from the processed differential GPS data and a density value of 2.67 g/cm^3 (which is the average density of crustal rocks) was used for intermediate layer reduction. The GRS 80 formula was used to reduce the data to the reference ellipsoidal surface whereas WGS 84 ellipsoidal reference system formula was used by the differential GPS to find the geographic coordinate of each gravity stations. As it was mentioned in chapter two, the difference between the two reference ellipsoid is very small and has negligible effect on the gravity survey.

The Bouguer anomaly generated was simple Bouguer anomaly since the terrain reduction was not carried out. This is because the area has not as such rugged topography and the 90 meters DEM model available for this work would have caused more damage than improvement. It is also believed that the gently varying topography would have a linearly varying effect that can be filtered easily. Therefore, it is preferred to filter possible linear terrain effect using data filtering techniques.

The simple Bouguer anomaly was then further processed to separate the residual from the regional effects to come upon with the residual and regional anomalies. This was necessary not

only to remove unaccounted linear effect during data reduction but also to separate short wavelength gravity effect(due to shallow structures which is important for this work) from long wavelength gravity effects (due to deep seated structures). For this work, both first and second order polynomial surface were fitted to the simple Bouguer anomaly using the program POLFIT (Lewi,E.,1997) and the fitted surface was considered as the regional anomaly while the difference between the Bouguer anomaly and fitted data was taken as the residual anomaly. Finally, the mapping software called Surfer8 was used to obtain different anomaly maps and modeling software called Grav2dc was used to model the subsurface using the residual anomaly along two profiles.

3.3.5 Error Analysis

The accuracy of the Bouguer anomaly is determined by the amount of errors which were propagated from the measured value to the Bouguer anomaly. Errors on Bouguer anomaly arise from the precision in determining latitude, height, reduction density, observed gravity and accuracy of instruments used in the survey.

The Bouguer anomaly in eq (46) is as a function of $(g_{obs}, h, \sigma, \phi)$. Assuming these Variables are independent and also their uncertainties are independent and random, the uncertainties propagated in the Bouguer anomaly (δg_{SBA}) is calculated by

$$\delta g_{SBA} = \sqrt{\left(\frac{\partial g_{SBA}}{\partial g_{Obs}}\delta g_{Obs}\right)^2 + \left(\frac{\partial g_{SBA}}{\partial h}\delta h\right)^2 + \left(\frac{\partial g_{SBA}}{\partial \sigma}\delta \sigma\right)^2 + \left(\frac{\partial g_{SBA}}{\partial \phi}\delta \phi\right)^2} \qquad (47)$$

(Taylor, J.R., 1997). Where δg_{Obs}= gravity observation errors, δh= height errors, $\delta \sigma$= density error and $\delta \phi$= latitude errors.

The observational gravity errors which were introduced in to the Bouguer anomaly can be computed by taking the first term of the partial derivative of equation (47) as follows

$\left|\frac{\partial g_{SBA}}{\partial g_{Obs}}\right| \delta g_{Obs}$ =10.6 μgal which is the overall accuracy of the gravimeter readings in this survey (δg_{Obs}). Therefore, an error of 10.6 μgal gravity value was introduced in to the

Bouguer anomaly due to errors in the observed gravity value. Similarly, by taking the second term of the partial differential of equation (47) and substituting the Bouguer anomaly equation in place of Δg , the error introduced in to the Bouguer anomaly due to height error is calculated as

$\left|\frac{\partial g_{SBA}}{\partial h}\right|\delta h$ = (0.3086-0.041925xσ) δh. The maximum accuracy in the measurement of height that was obtained after processing the DGPS data was δh = 0.00534m. Using this value and the Bouguer slab density (σ=2.67g/cm^3) in the above equation, an error of (0.3086-0.041925x2.67) x0.00534 (mgal) =1.05 μgal gravity value was introduced in to the Bouguer anomaly due to height determination error. The error introduced in to the Bouguer anomaly due to errors in density determination which was used for intermediate layer reduction (σ =2.67g/cm^3) is given by

$\left|\frac{\partial g_{SBA}}{\partial \sigma}\right|\delta\sigma$ = (0.041925xh) $\delta\sigma$.The accuracy in determining the density of intermediate layer is not known because, the density used for such purpose was the average crustal density of the rocks which may or may not differ from the averaged density of the intermediate layer for the study area. If we assume that the average crustal rocks density value (2.67g/cm^3) is different from the average density of rocks found in the locality or used in the intermediate layer reduction, the value of $\delta\sigma$ will be different from zero but not known for this time, or if we assume that the average crustal rocks density value (2.67g/cm^3) is equal to the average density value of the intermediate layer, $\delta\sigma$ will be zero which is not reliable. For simplicity if we consider the second cause where $\delta\sigma$=0, then the error introduced into the Bouguer anomaly due to intermediate layer reduction density determination will be equal to zero.

Using the last term of eq (47) and differentiating the Bouguer anomy with respect to latitude (i.e. the normal gravity formula GRS 80 of equation 35), the error introduced in to the Bouguer anomaly due to errors in latitude determination is given by

$\left|\frac{1}{R_E}\frac{\partial g_{SBA}}{\partial \phi}\right|\delta\phi$. Then substituting the value $\delta\phi$= 0.00287meter which is the minimum latitude error that we got from the DGPS data, $\phi = 4.599127^0$ the mean latitude of the study area and R_E =6371008.7714m the mean radius of the earth, the error introduced into the Bouguer anomaly due to errors in latitude determination is

$\left|\frac{1}{R_E}\frac{\partial g_{SBA}}{\partial \phi}\right|\delta\phi$= $(1.296\text{x}10^{-4})\delta\phi$= $(1.296\text{x}10^{-4})$ x0.00287(mgal)=0.37 μgal. Therefore, the error that was introduced in to the Bouguer anomaly due to the measurement in the uncertainty of latitude is 0.37 μgal.

Taking into account all the above errors, the total amount of random errors introduced in to the Bouguer anomaly is computed by using equation (47) as follows

$$\delta g_{SBA} = \left[(10.6)^2 + (1.05)^2 + 0 + (0.37)^2\right]^{1/2} x10^{-6} = 10.66\ \mu gal \qquad (48)$$

This is the maximum accuracy obtained using minimum error values for $h, \sigma,$ and ϕ. If we consider the maximum error value for h and ϕ, the total amount of random errors introduced in to the Bouguer anomaly will be 11.46 μgal which is very small value.

3.3.6 Reliability of Gravity Reductions.

The raw gravity values and height are negatively correlated with the square of the Pearson correlation coefficient being 0.9297. As we can see from Figure 3.3 below, the regression using the least square approach showed that 92.97% of the raw gravity value is explained by the height.

Figure 3.3 Graph of raw gravity versus Height.

Though the free-air correction has reduced the correlation between the gravity anomaly and the height, 76.54% of it is still being accounted for the height. That means only 16.43% correlation in the raw gravity was removed. As it can be seen from the Figure 3.4, the positive correlation is also to be expected after the free-air reduction. This strong linear correlation between the two values confirms that the spatial data reductions (latitude and height) have been done successfully.

The Bouguer anomaly has leas correlation with height. Figure 3.5 shows the square of the linear correlation coefficient between the two values is 0.0545. The correlations observed in the raw gravity (92.72%) or in the free air anomaly (76.54%) with height are removed in the case of simple Bouguer anomaly. As it was explained in the 3.3.4 gravity data processing subtopic, the value of the density used for the intermediate layer reduction was 2.67g/cm^3, which is the average density of crustal rocks. When one analyzes this correlation value from the perspective of correlation analysis, it is negligible. However, even if there is a doubt, it might been caused either due to minor adjustment to be applied to the density used for intermediate layer reduction, or because of some compensating signal or due to unapplied terrain reduction. Therefore, the negative correlation with the height might be the sum effect of the density used, compensating signal and the terrain effect. However, since the correlation is negligible, any

further processing of the data using the available digital elevation models to further remove topographic effects will harm the result more than it improves.

Figure 3.4 Graph of Free-air anomaly versus Height.

Figure 3.5 Graph of Bouguer anomaly versus Height.

Further improvement of local anomaly can be achieved by removing the regional signal from the Bouguer anomaly to get the residual effect. For this case, first and second degree

polynomial surfaces are fitted to the Bouguer anomaly. Then the correlation of the residual and regional anomalies to the topography is checked as shown in Figures 3.6, 3.7 and 3.8.

The residual anomaly (first degree) is less correlated to the topography whereas the regional anomaly (first degree) is more correlated to the topography. This is a good indication that the regional anomaly is due to deep seated structure, which is part of the un-removed topographic related signal that might be related with the compensational signal. This assumption is especially well reflected when we see that the residual (first degree) anomaly, in which only 0.82 % of it is accounted for the topography and the other 99.18% of the anomaly is related to the subsurface geologic features whereas 70.89% of the corresponding regional anomy is negatively correlated to the height.

The small negative correlation with height seen in the simple Bouguer anomaly is removed in the first degree residual anomaly. Like the first degree, the second degree residual anomaly (Figure 3.8 **a**) has 0.23 % correlation to the height which is very small correlation and the corresponding regional anomaly has also very small (7.72%) correlation to the topography.

Figure 3.6 Graph of First degree Residual anomaly versus Height.

Figure 3.7 Graph of First degree regional anomaly versus Height.

Figure 3.8 Graph of second degree Residual (a) and Regional (b) anomalies versus Height.

CHAPTER FOUR

RESULTS, DISCUSION AND INTERPRETATION

4.1 Results and Discussion of different anomaly maps

The outputs of the geophysical data were used to produce different anomaly maps which show contrast in the resistivity and density of the subsurface rocks. In this work, the VES and gravity together with DGPS data were used to produce maps and examine the relative contrast in resistivity and density of the subsurface rocks. In order to study the contrasts in resistivity and density of the subsurface rocks; plots of pseudodepth sections and gravity profiles (second degree residual gravity anomaly versus distance) along two survey lines, apparent resistivity sliced pseudodepth map of the study area for six current electrode spacings, free-air, Bouguer, residual and regional gravity anomaly maps were prepared and presented in this section.

4.1.1 Apparent Resistivity Maps and gravity profiles

The apparent resistivity data from different VES points at current electrode spacing AB/2=9m was taken to produce the apparent resistivity plan map of the area shown in (Figure 4.1). This map shows the apparent resistivity of the area at shallow depth. The central-northern part of the area shows high apparent resistivity value ranging from 240-600 Ohm-m bounded by the low apparent resistivity values. The high apparent resistivity value zone has NNW-SSE trend, with a NNE-SSW trending interruption in the south. This high apparent resistivity value extends to the central part of the area up to L4-V3. The low apparent resistivity value from 0-40 Ohm-m covers the west, southwest and northeast parts of the area. The transition zones separate the high apparent resistivity zones from the low apparent resistivity zones.

The first transition zone extends from northeast and passes through Line-8 VES-3(L8-V3), L5-V1, and L6-V2 then terminates to the east of L6-V2 in northeast trend whereas the second transition zone starts from northwest part and passes through L2-V2, L8-V6, L5-V5, L6-V3 and terminates with southwest-northeast trend. The southeastern corner of the area shows relatively high apparent resistivity and seems to be the continuation of the northern high resistivity zone.

In order to see how these high and low apparent resistivity zones behave at depth along the profiles and in the whole area, pseudodepth sections along survey Lines-6 and 8, and apparent resistivity sliced pseudodepth map of the study area were prepared.

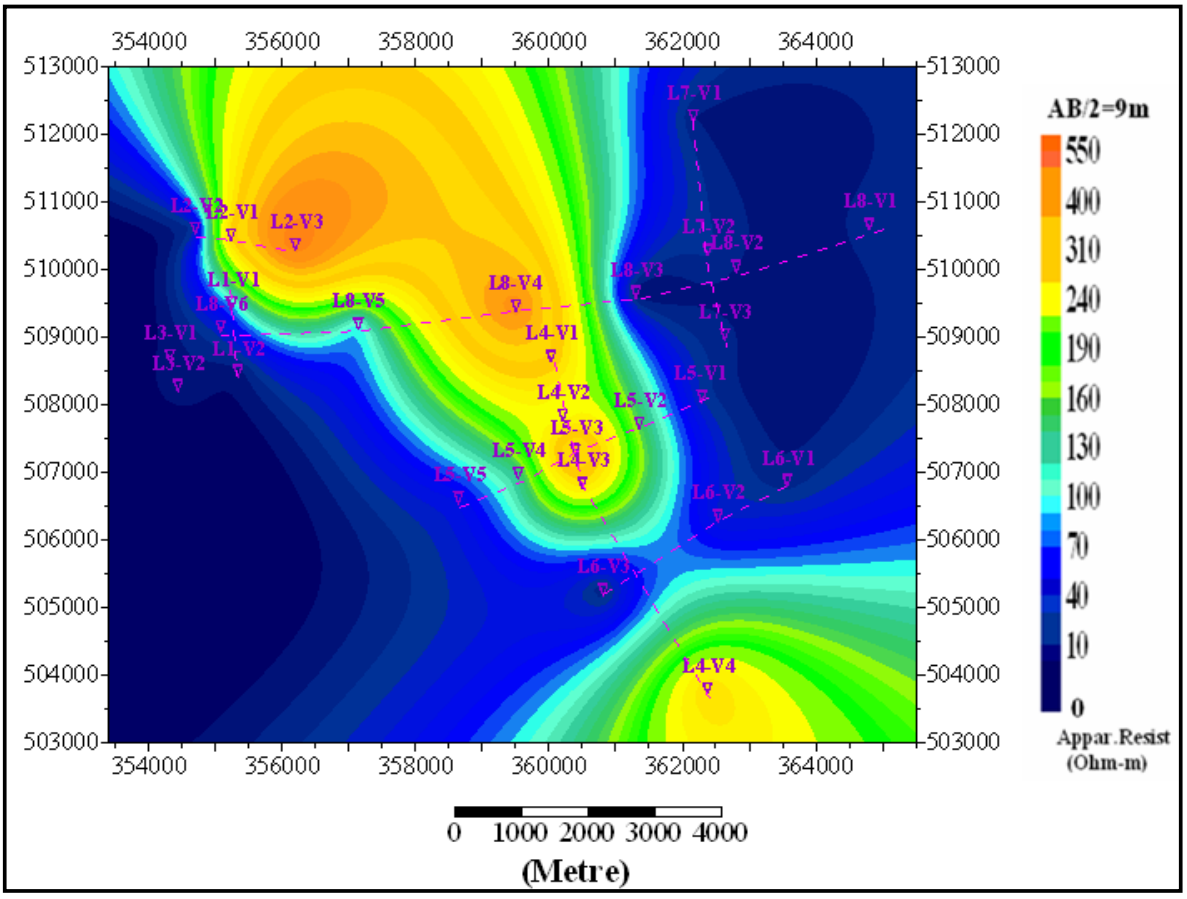

Figure 4.1 Apparent resistivity Plan map for current electrode spacing AB/2=9m.

A) **Apparent Resistivity Pseudodepth Section and residual gravity profile along Survey Line-8(V1-V6)**

The apparent resistivity pseudodepth section along Line eight (Figure 4.2) indicates wide variation of apparent resistivity values ranging from 0-290 Ohm-m. A continuous and vertically extending low apparent resistivity anomalous zone with values from 0-70 Ohm-m is observed beneath L8-V3. This anomalous zone is extending to the east at shallow depth towards L8-V2 and L8-V1. A similar but very shallow depth low resistivity zone is observed in the west beneath L8-V6. The apparent resistivity values beneath L8-V1 and L8-V2 increases with depth

but below L8-V3, continues as low apparent resistivity as depth increases up to a pseudodepth of 1000m.

The gravity profile plot along this survey line (Figure 4.2) shows the variation of second degree residual gravity anomaly with distance from west to east. As it can be seen from Figure 4.2, intermediate residual gravity anomaly is observed beneath L8-V6, L8-V5 and near to L8-V4 but high residual gravity anomaly peak between L8-V4 and L8-V3. The residual gravity value shows drastic change (decreases rapidly) starting from L8-V3 to the east towards L8-V2 and attains its lowest value around L8-V1.

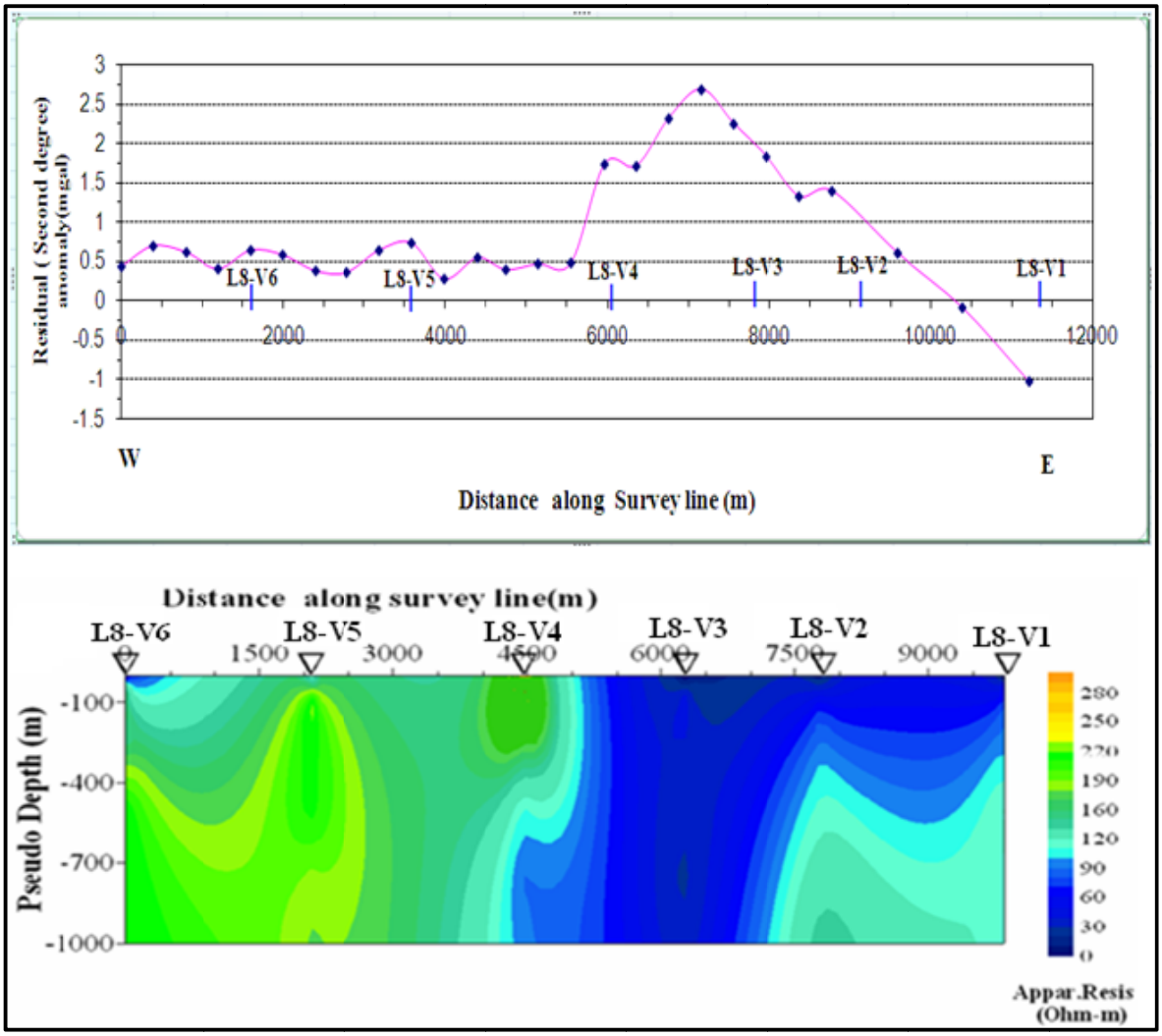

Figure 4.2 Apparent resistivity pseudodepth section and gravity profile plot along Line-8.

B) Apparent Resistivity Pseudodepth Section and gravity profile along Survey Line-6(V1-V3).

The apparent resistivity pseudodepth section along Line six (Figure 4.3) shows apparent resistivity values ranging from 0-190 Ohm-m which is less in magnitude compared to that obtained in survey Line-8. The low apparent resistivity values beneath the three VES points observed in Figure 4.1 are observed to remain shallow in this pseudodepth section as well. The apparent resistivity value beneath L6-V3 varies from 0-100 Ohm-m which is low as compared to that on L6-V2 and L6-V1 where the apparent resistivity value varies from 0-180 Ohm-m.

The gravity anomaly plot along this survey line (Figure 4.3) shows an increase from west to east. As it is shown in this figure, the lowest residual gravity anomaly is observed between L6-V3 and L6-V2, which is also shown as low apparent resistivity value in the pseudodepth section. The value of the residual gravity anomaly increases smoothly from L6-V2 towards L6-V1, where alternatively higher resistivity anomaly is observed at depth.

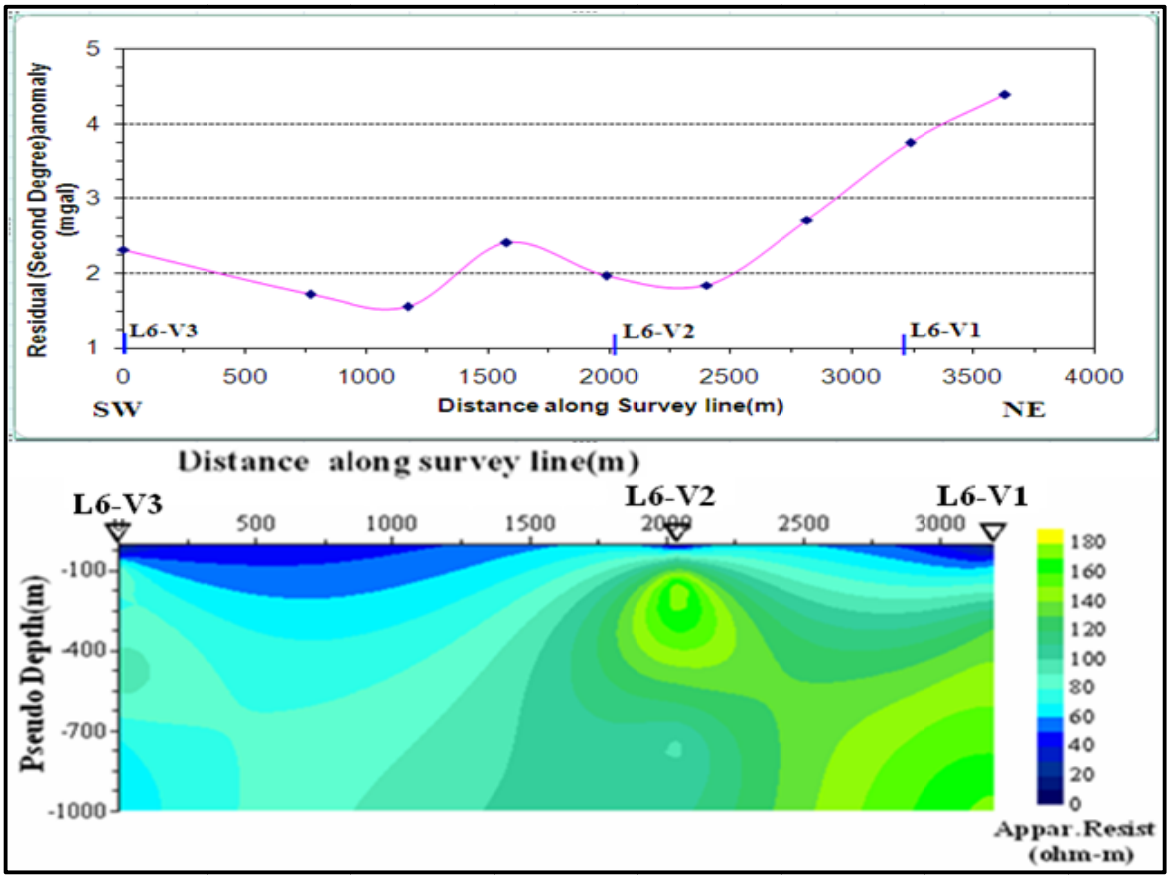

Figure 4.3 Apparent resistivity pseudodepth section and gravity profile plot along Line-6.

C) Apparent Resistivity Sliced Pseudodepth Map

The apparent resistivity sliced Pseudodepth map (Figure 4.4) was prepared by superimposing the two dimensional apparent resistivity plan maps for six different current electrode spacings. This map shows the relative variation of the apparent resistivity value of the whole area laterally as well as vertically at different pseudodepths. The apparent resistivity value varies from 0-800 Ohm-m. The amplitude of the high apparent resistivity value zone (Figure 4.1), decrease as the investigation depth increase. The amplitude of the very low apparent resistivity zones observed in the northeast and southwest parts of the area (Figure 4.1) increases as depth increase. The apparent resistivity value around southeast corner of the area increase in both amplitude and areal coverage to the pseudodepth of AB/2=45m and decrease until AB/2=500m and finally starts to increase again to pseudodepths of AB/2=750m and 1000m. Similarly, the apparent resistivity value of the area found south of VES point L5-V5 and southwest of VES point L6-V3 increase to AB/2=100m and decreases again at AB/2=750m and 1000m.

The apparent resistivity value of the three transition zones (Figure 4.1) increase with depth except in the region of VES point L8-V3 which continues as a low apparent resistivity value to pseudodepth of AB/2=1000m.

4.1.2 Gravity Anomaly Maps

A) Free-Air Anomaly and Topography Maps

Figure 4.5**a** shows the topography of the survey area and (**b**) the free-air anomaly. The value of the free-air anomaly varies between -18mgal to -7.3mgal whereas the height of the area varies between 1050m to 1135m in reference to WGS84 reference ellipsoid. The free-air anomaly map was plotted with a contour interval of 0.25mgal and the topography map with 3m contour interval by using surfer8 mapping software.

The strong positive correlation between free-air and height is explained in chapter three by using graphs. Figure 4.5 shows the relative variation of the two values in the area. Their value varies from low in the western to high in the eastern part of the area. The height value increases from northwest to northeast and the free-air anomaly follows similar trend but

difference in that its highest value is concentrated at the central-eastern part of the area with northwest-southeast trend.

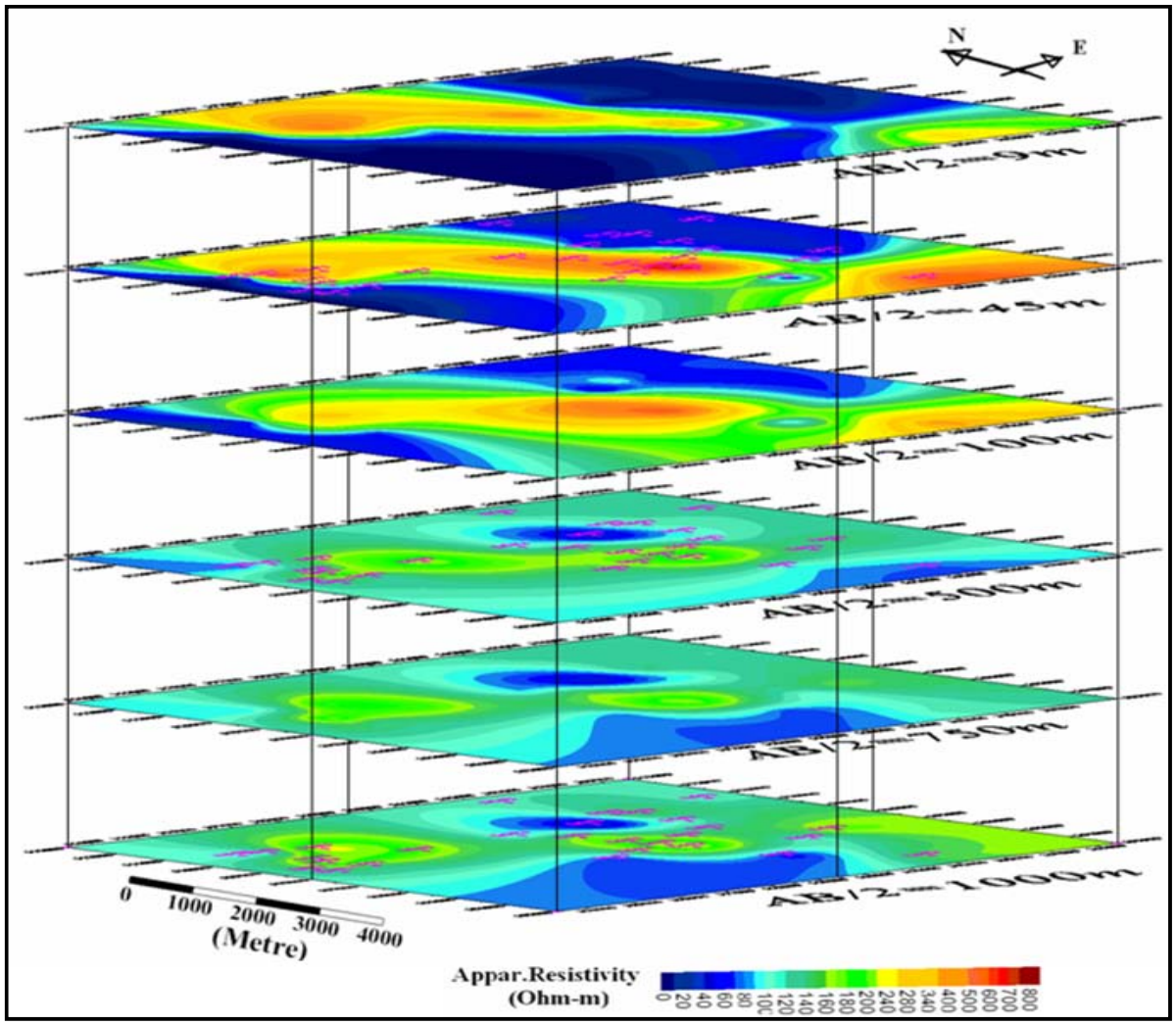

Figure 4.4 Apparent resistivity sliced pseudodepth map.

B) Bouguer Anomaly Map

The Bouguer anomaly map of the study area (Figure 4.6) is the result of Bouguer reduction in which the topographic effect was minimized. It has a contour interval of 0.2mgal and its value varies from -11.6mgal to -6.47mgal. The low Bouguer anomaly value (-11.6 to -9.4 mgal) is observed in the northeast, south and southeast parts whereas high Bouguer anomaly value (-8 to -6.47mgal) is observed in the west and east parts of the area.

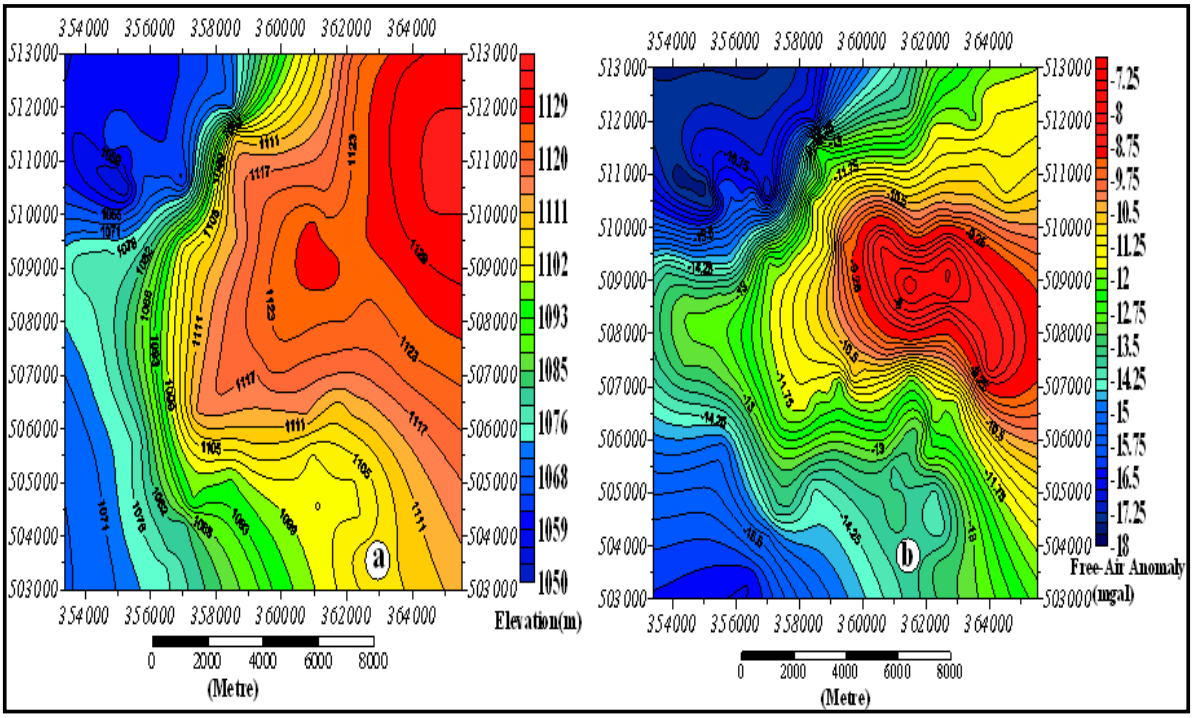

Figure 4.5 Comparison between topography map (a) and free-air anomaly map (b).

The high free-air anomaly value which is observed in the eastern part of the free-air anomaly is also seen in the Bouguer anomaly, but with broader area coverage and higher intensity. It has a similar trend with that in the free-air anomaly. The low Bouguer anomaly value in northeast, south and southeast parts of the area are seen as high value in the free-air anomaly. This shows that these values in the free-air anomaly are affected by the high topography and the related Bouguer plate. The northwest and southwest corners of the area have medium to high Bouguer anomaly values which are seen as low in the free-air anomaly due to the low topography.

C) Residual Gravity Anomaly Maps

The residual gravity anomaly maps which are shown below in Figures 4.7 and 4.8 were produced by fitting first and second degree (linear) polynomials to the Bouguer anomaly data respectively.

The first degree residual gravity anomaly map shown in Figure 4.7 below has a contour interval of 0.2mgal and its value varies from -2.2 to 3.2mgal. It has the lowest anomalous value in the northeast and lower residual anomalous value in the south parts of the area which are also observed in the Bouguer anomaly. The high anomaly values in the west and east part of the area

are also observed in the Bouguer anomaly with little modification in their relative values but with the same trend whereas the northwest part of the area shows low residual anomaly value which is seen as a medium to high in the Bouguer anomaly map. This shows that the very low and high anomaly zones in the Bouguer anomaly maps are less affected by the compensational signal effects relative to the medium or northwest part.

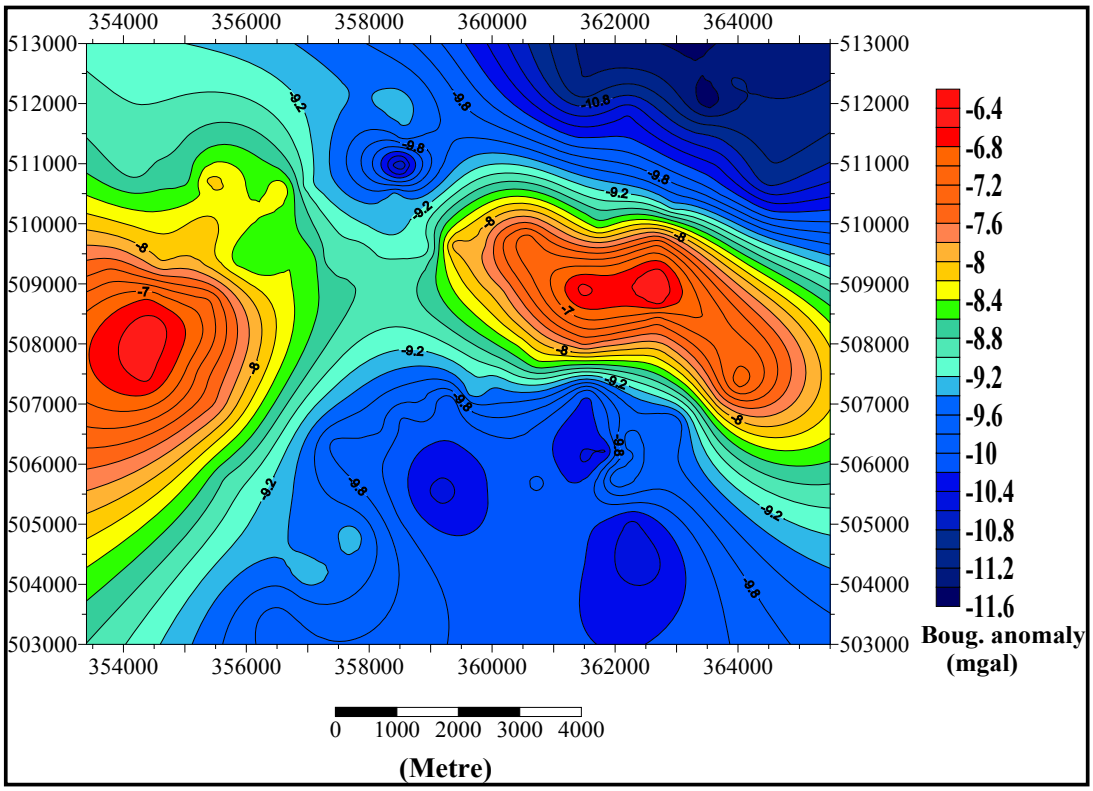

Figure 4.6 Bouguer anomaly map.

The very low residual gravity anomaly zone in the northwest part has a close proximity with the Bouguer anomaly map of the study area of the same locality. The resemblance of these parts in the Bouguer anomaly and residual anomaly as a result of the first degree polynomial fitting shows that this zone is not highly affected by the regional effect.

The low and medium anomaly zones shown as blue and cyan color contour lines which cover the northern and southern part of the area in the residual anomaly map (Figure 4.7) have only little resembles to the Bouguer anomaly map in the southern and northeast part of the area. The high anomaly zones in the west and east part of the area shown in residual anomaly map are also seen as high in the free-air and Bouguer anomaly maps.

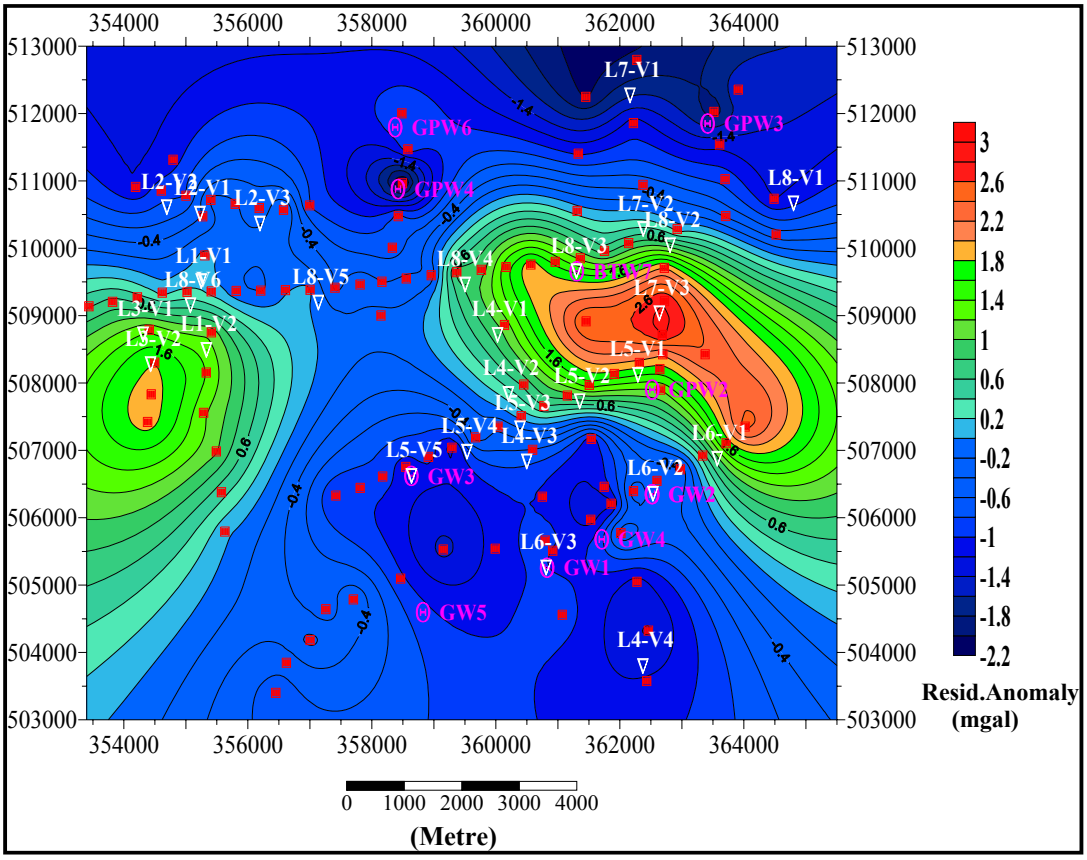

Figure 4.7 First degree polynomial surface fitting Residual anomaly map.

The second degree residual gravity anomaly map (Figure 4.8) has a contour interval of 0.2mgal and its value varies from 0.8 to 5.2mgal. It has very low anomaly zone in the northeast part of the area which is similar to Bouguer anomaly. The high anomaly values in the western and eastern parts of the area are also observed in the Bouguer anomaly and first degree residual anomaly maps with little modification in their size, shape and amplitude but with the same trends. This shows that these high anomaly zones are affected by dens materials underneath. Unlike the other previous maps, the northern part of the area shows medium to high residual anomaly values which might be due to the presence of high dens rocks at shallow depth. Similar cause are observed in the south part of the area which shows high in the second degree residual anomaly and low in the case of Bouguer and first degree residual anomalies.

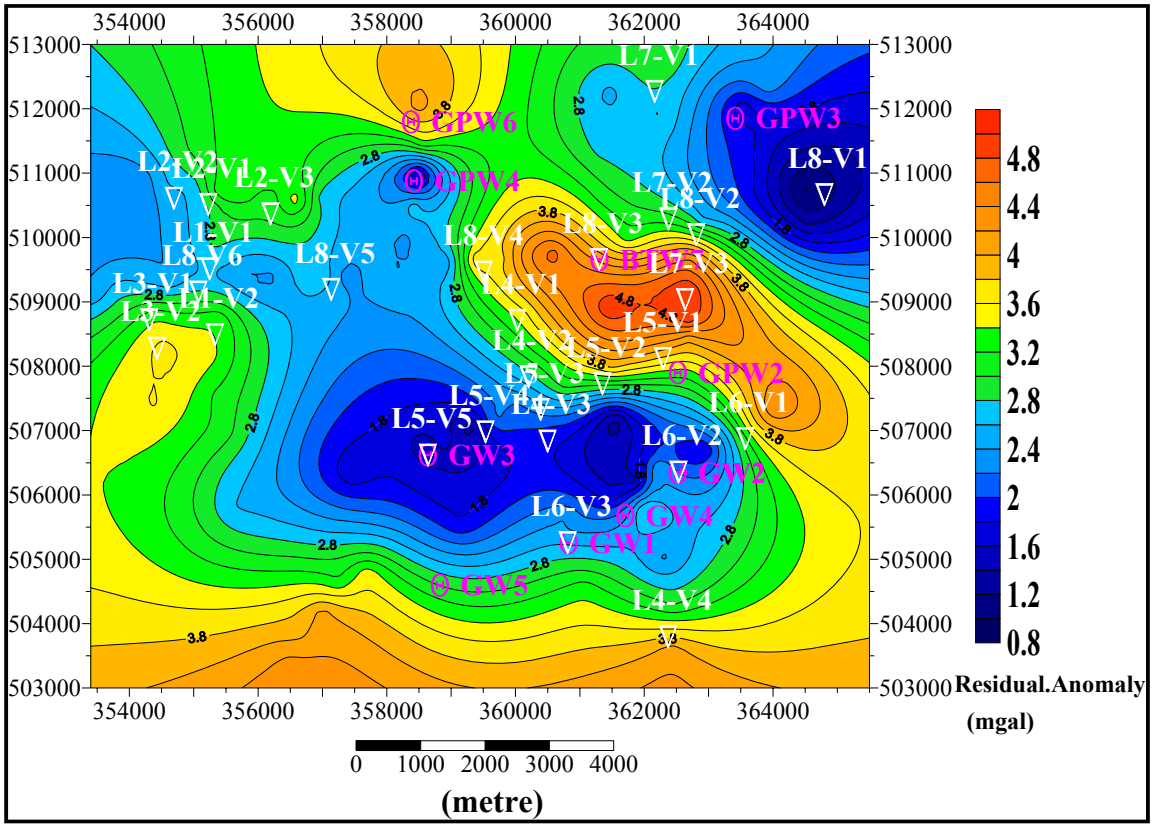

Figure 4.8 Second degree polynomial surface fitting Residual anomaly map.

D) Regional Gravity Anomaly Maps

The regional gravity anomaly maps (Figure 4.9 **a** and **b**) were produced by first degree(a) and second degree(b) polynomial surface fitting to the Bouguer anomaly. The first degree regional anomaly map (Figure4.9 **a**) has a contour interval of 0.1mgal and a range of values between -9.8 to -7.6mgal. It has low regional anomaly value at the north-eastern part of the area, which is seen as high topography in the topographic map. Similarly, the high anomaly value in the north-western part of the area is reflected as low topography in the topographical map (Figure 4.5 **a**). This clearly indicates that the regional anomaly is the reflection of the compensational signal and its effect is removed in the regional- residual separation. Generally, the regional anomaly value increases smoothly from west to east which is the reverse to the topography and the contour lines move from south to north directions with a linear trend.

The second degree regional anomaly map (Figure4.9 **b**) has a contour interval of 0.2mgal and a range of values between -14.6 to -9.6mgal. It has low regional anomaly value at the north and south parts and high regional anomaly value in the west part of the area.

Even if the corresponding residual anomaly shows low correlation to the topography which indicates the removal of compensational signal effects, the regional anomaly map shows relatively lower correlation to the height. This might be considered as an indication that some part of the residual signal is included in the regional part.

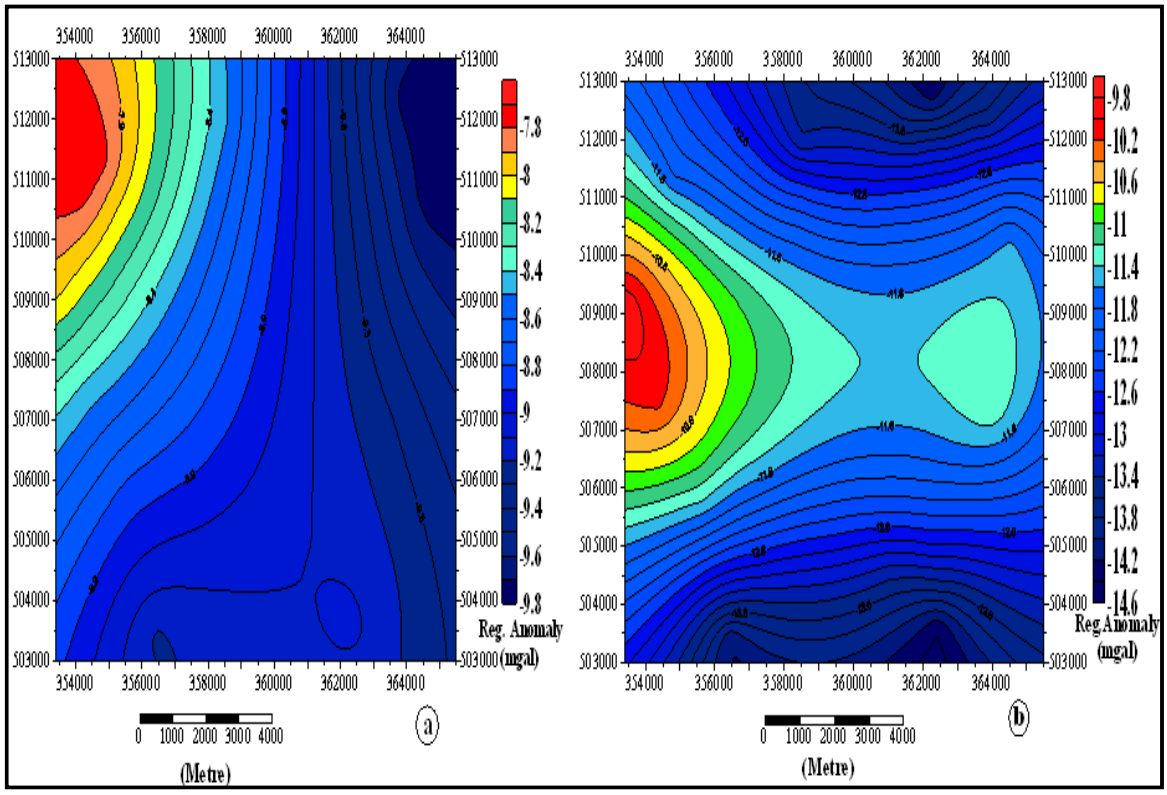

Figure 4.9 Regional gravity anomaly maps for first degree (a) and Second degree (b).

4.1.3 Basement topography map

The basement topography map of the area (Figure 4.10) was produced by using the depths to the basement, based on data from ten boreholes. The locations of these boreholes in the area are shown on the map. This basement map has a contour interval of 4m and a range of values between -200m to -120 m. The map shows that the basement is mate at deeper location (168-200m) in central part of the area which includes GW3, GW1, GW4 and GPW2. The north-west and the southwest parts of the area (where GPW4, GPW6 and GW5 are found) show the basement is found at shallow depth with value range of 130-113m. The deepest locations of the basement are observed at GW3 and GPW3.

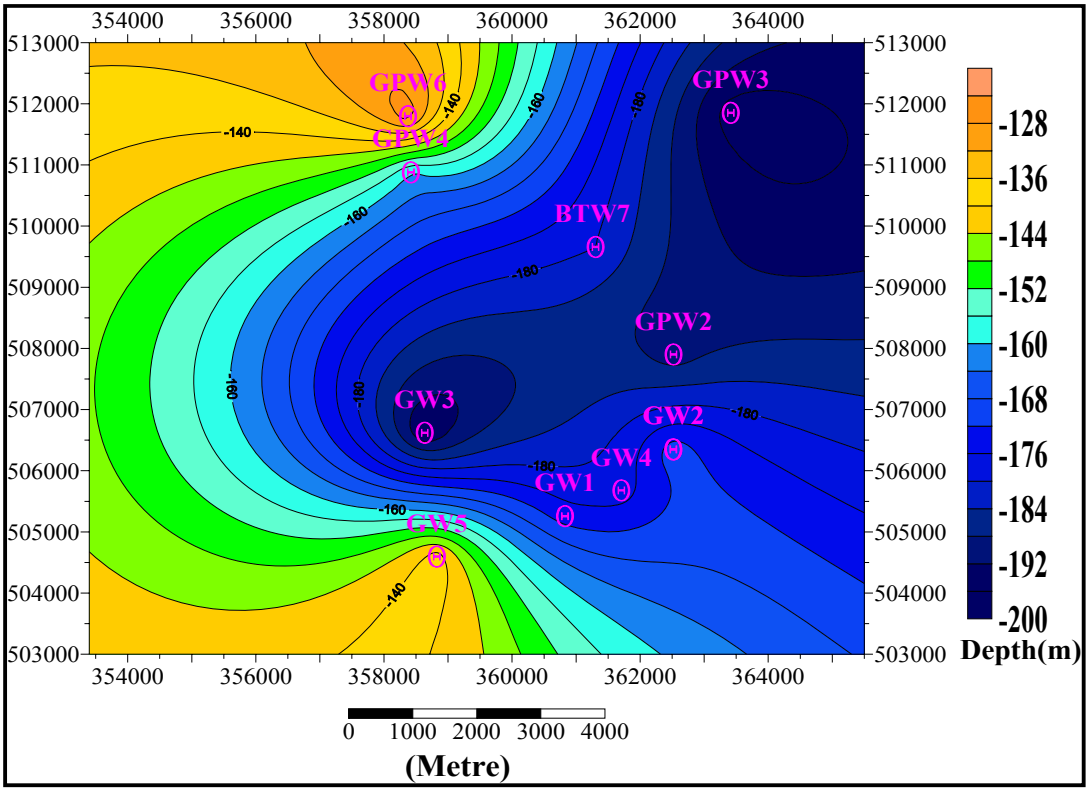

Figure 4.10 Basement topography map.

4.2 Qualitative Interpretation

For convenience, names are assigned for the three resistivity zones shown in the apparent resistivity map (Figure 4.1) in order to correlate them with what is observed in the other apparent resistivity, gravity and geological maps.

Zone I is the high apparent resistivity zone in the area, zone II is including all low apparent resistivity zones while Zone III is the transition between Zone I and Zone II. Therefore, the interpretations of the three regions will be made separately by correlating with other resistivity, gravity and geological maps in order to have a better picture of them.

Zone I

This high anomaly zone at shallow depth is correlated to be the quaternary vesicular basalts and crossed by the alluvial deposit in the northern part of it in northeast-southwest direction shown in the geological map of the area (Figure 1.2). The apparent resistivity value of this zone

decreases as depth increase (Figure 4.4). This can be also seen in the Pseudodepth section of Line-8 (Figure 4.2). The decrease in the apparent resistivity of this zone as depth increases might be due to the weathering and fracturing of the rocks and possible presence of water saturated zones that overlay the high resistive basement.

This zone is crossed by two week zones (considered as faults after referring to the surface geology). The first fault line runs from north-central part to south-western part of the area. On the other hand the second fault line starts from the north-central part of the area near to the first fault line and runs to the south-east. The two fault lines cross each other outside, but near to the study area, which is shown in the geological map of Gelchet area (Figure1.2). The first fault line cross line-8 around L8-V5 and second fault line cross this profile around L8-V3.

These faults are clearly seen in all the Bouguer anomaly, first degree residual gravity anomaly and second degree residual gravity anomaly maps. The apparent resistivity plan map for AB/2=1000m has the alignment of contour lines along the fault path only within a few places in this zone. These faults are most probably used as a path for the ground water movement towards the low basement topography regions. Therefore, the boreholes drilled near to the first fault line (GPW4 and GPW6) where the basement topography is high are dry. The second fault line is crossed by massive basalt which is found above the basement to the southeast of L8-V3. The basement topography and second degree residual anomaly maps show that the depth to the basement increases along the second fault line until it is crossed by the massive basalt. The water which flows following the basement topography along this fault line has a tendency to be accumulated around L8-V3. As a result of this, the borehole (BTW7) drilled around L8-V3 has groundwater yield of greater than 5.6 l/sec.

Zone II

The very low apparent resistivity zone with apparent resistivity value (0-40Ohm-m) in the northeast, west and southwest parts of the area (Figure 4.1) is covered by quaternary vesicular basalts (Figure 1.2). The northeast part is topographically the highest in the study area (Figure 4.5 **a**) with height value ranging from 1112-1132 m above WGS84 reference ellipsoid. The apparent resistivity of this area increases as depth increase (Figure 4.4). This is also seen in the pseudodepth section of survey Line-8 which crosses the northeastern part of this zone. As one can see from the pseudodepth section of this survey line (Figure 4.2), the contour colors are oriented horizontally and their value increases as depth increases beneath L8-V2 and L8-V1.

The gravity profile along this survey line shows that second degree residual gravity anomaly value decrease rapidly from L8-V3 towards L8-V1 and away from it. Similarly, the Bouguer anomaly and first degree residual gravity anomaly values decrease rapidly from L8-V3 towards L8-V1 and attain their minimum value to the east of L8-V1. The basement topography map (Figure 4.10) also shows an increase in the depth to the basement which shows that the gravity value of this part of the area is mostly affected by the density of the basement.

The Bouguer and residual anomaly maps (Figure 4.6, 4.7 and 4.8) show that the northeast part of this zone is crossed by high gravity anomaly body (most probably massive basalt) which is partially covered by high resistivity value (included in zone I) and partially by low resistivity value (included in zone II) as observed in apparent resistivity plan map for AB/2=9m (Figure 4.1). The massive basalt covers the southern part of this zone starting from L6-V2 and extends to the north by crossing Line seven in between L7-V2 and L7-V3 and Line eight in between L8-V3 and L8-V2 in the northwest-southeast direction. The apparent resistivity value of this zone continues as low to the pseudodepth of AB/2=100m and later increase to the pseudodepth of AB/2=1000m (Figure 4.4). The apparent resistivity value of northeast corner of this zone (near but to the east of GPW3) starts to decrease at pseudodepth of AB/2=1000m which is also seen in second degree residual gravity anomy map (Figure 4.8). The borehole (GPW3) drilled in this zone has a total ground water yield of 3 l/sec which is a very small magnitude as compared to GW1 and GW2. This might be due the absences of bounded low topography basement.

The very low apparent resistivity value which covers the west and southwest parts of the area (Figure 4.1) increases in amplitude but decrease in areal coverage as depth increase (Figure 4.4). The western part of the area is covered by quaternary vesicular basalt (Figure 1.2) shown as high gravity value having southwest-northeast trend bounded by the alluvial deposit from the north and fault line one from the east. The northwestern part of the area which is represented by low topography and low free-air anomaly (Figure 4.5 **a** and **b**), high first degree regional anomaly (Figure 4.7) shows low apparent resistivity value for both shallow and high depths (Figure 4.4). It is bound by high density value from the south (Figure 4.8) and crossed by the alluvial deposits in between L2-V2 and L2-V1 (Figure1.2). The second degree residual gravity anomaly map (Figure 4.8) shows a decrease in its value to the west of L2-V2. The smooth color contour transition from low to high in the second degree residual gravity anomaly map also in

the apparent resistivity plan maps at different pseudodepths (Figure 4.4) near to L2-V2 might be caused by a structure, which was not identified in the geological map.

The low second degree residual anomaly values near to L5-V5, L4-V4 and L6-V3 are also low in the basement topography maps. This zone is believed to be a good ground water potential zone and the drilled boreholes in this zone after the recommendation of this survey; GW1 around L6-V3 has ground water yield of greater than 17l/sec, GW2 around L6-V2 has a yield of greater than 15 l/sec, GPW2 located near to L5-V1 and on the transition zone in the second degree residual anomaly map has a yield of 3 l/sec. This value is smaller than other well yields value because GPW2 is located at higher apparent resistivity value zone and where the gravity value is increasing to very high gravity anomaly value. The places having low second degree residual gravity value, low apparent resistivity value at AB/2=750 and 1000m which are found to the south of L5-V5, and near to L2-V2 are suggested to be good places for ground water extraction.

Zone III

The transition zone between Zone I (high apparent resistivity zone) and Zone II (low apparent resistivity zone) has three clear orientations in the apparent resistivity plan map (Figure 4.1). The first part of this zone pass through L2-V2, L8-V6 and L6-V3 in the northwest-southeast direction by separating the low apparent resistivity value found in the west and south of the area from the high apparent resistivity value found to the northeast of this zone. The second part of this zone pass through L8-V3, L5-V1 and L6-V2 in the NE-SSW direction by separating the high apparent resistivity zone found to the west of it and low apparent resistivity zone found to the north and east of it. The third part of this zone passes though L6-V3 and L6-V2 by separating the high apparent resistivity values found in the north and southeast corner of the area. The apparent resistivity value for both parts of this transition zone increases as depth increase (Figure 4.4). Neither of these parts of the transition zone is defined by the gravity or geological maps as a transition zone or structures. Therefore, they are related to shallow depth structures most probably caused by weathering which disappear within a certain shallow depth.

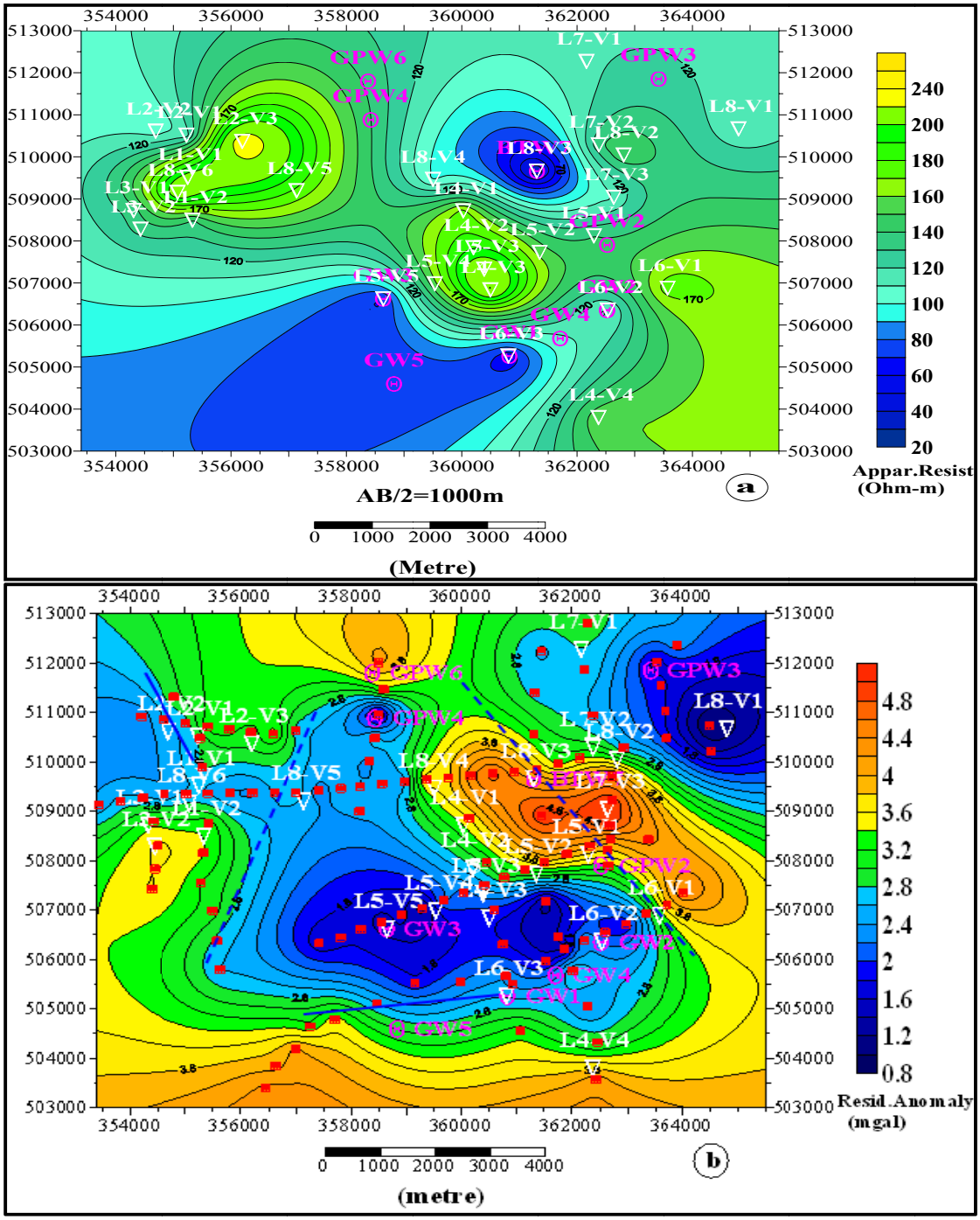

Figure 4.11 Comparison between apparent resistivity plan map for AB/2=1000m (a) and second degree residual gravity anomaly map (b).

4.3 Quantitative Interpretation

Quantitative interpretations of geophysical data were done by modeling the resistivity and gravity survey results along selected profiles. The results of resistivity modeling were presented

as geoelectric sections whereas the gravity modeling were presented as graphs showing the match between the modeled and residual anomaly in the top part and modeled subsurface in the lower part of the model. The elevation of each layer rather than depth was used during the construction of geoelectric sections. These results were helped to determine the depth to the aquifer and identify the different degree of weathered and fractured lithologic units as well as depth to the basement along profiles.

4.3.1 Geo-electric Sections

The final result from one dimensional inversion of VES data along two survey lines (Line-6 and 8) were used to construct the geoelectric sections in order to identify the distribution of different lithologic units in the vertical direction. The softwares which were used for the inversion of the VES data were Resix-Ip and WinResist whereas the plotting was carried out by using AutoCAD and later by using surfure8 software. The lithologic logs from boreholes that are lying on these profiles were used to fix the thickness of each layer by grouping the rock samples based on their type and degree of weathering and fracturing. The pseudodepth sections along these survey lines were examined to see the relative resistivity variations when preparing geoelectric sections.

A) Geo-electric section along Line-8(V1-V6)

The geoelectric section of Line eight (Figure 4.12) was constructed from the model parameters of VES points data found along Line-8(V1-V6). The borehole BTW7 located around L8-V3 was used to constrain (fix) depth for L8-V3 and later parameterize the resistivity values and depths of the other VES points using this value. Table 4.1 below shows the lithologic log of BTW7 which was used to fix the depth and type of layers when L8-V3 was modeled.

The geo-electric cross-section (Figure 4.12) indicates the shallow subsurface lithologic units in the study area which are represented by five major and two minor (having small thickness) geoelectric units.

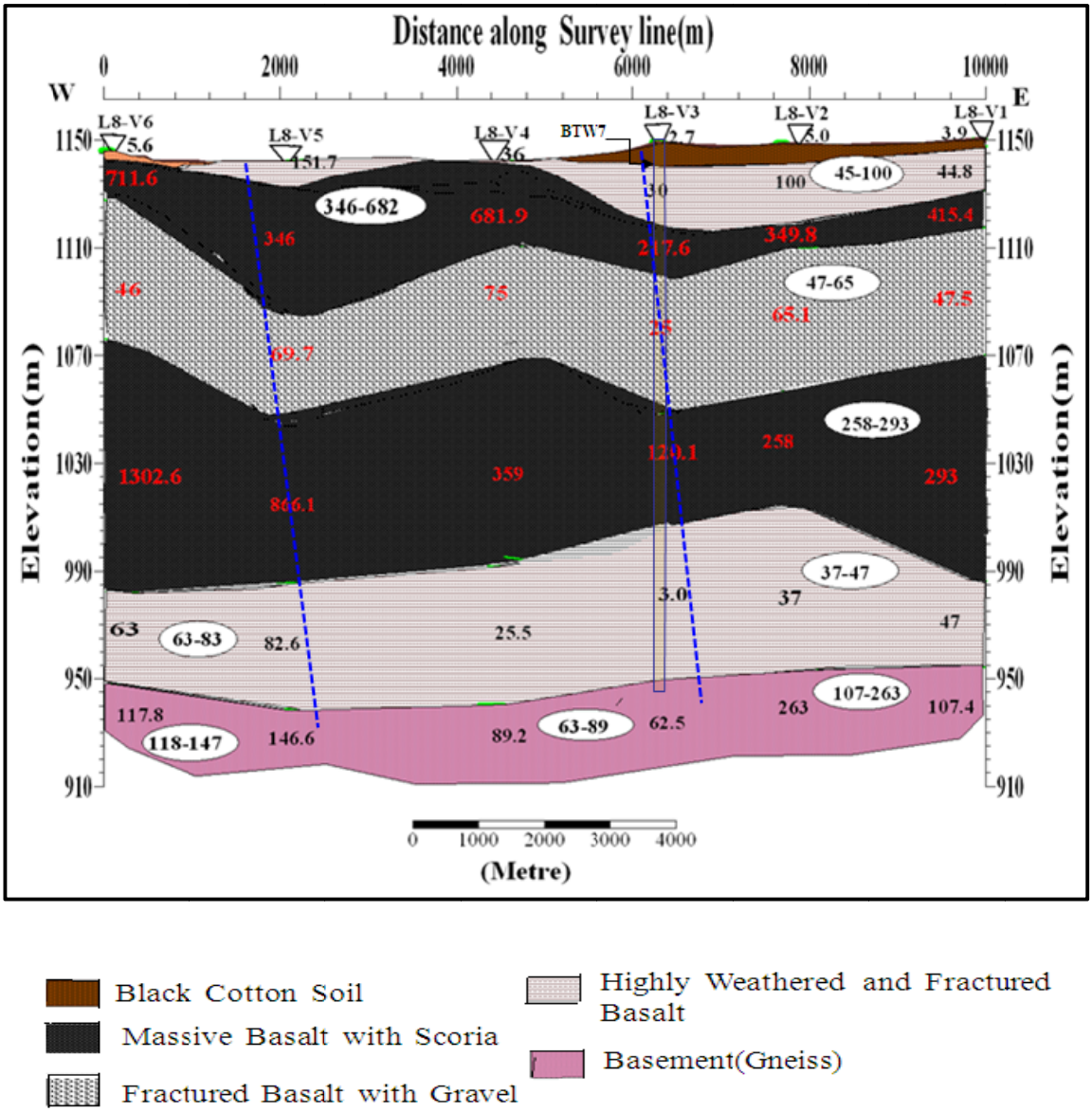

Figure 4.12 Geo-electric section along Line-8, Gelchet, Borena Zone.

The five major lithologic units have relative resistivities in accordance with the following patterns; $\rho_3 > \rho_4 < \rho_5 > \rho_6 < \rho_7$ and the relative resistivities of two minor lithologic units are $\rho_1 < \rho_2$. Where ρ_3 with resistivity value from 217-711.6 Ohm-m, ρ_4 (25-75 Ohm-m), ρ_5 (120-1302.6 Ohm-m), ρ_6 (3-82.6 Ohm-m) and ρ_7 (62.5-263 Ohm-m) are the resistivities of upper massive basalt with scoria (overlaid by highly weathered and fractured basalt and cotton soil), fractured basalt with gravel, massive basalt with scoria, highly weathered and fractured basalt and basement (gneiss) respectively.

Table 4.1 Lithologic log of borehole BTW7.

Lithology	Depth(m) from the surface
Black cotton soil	0-6
Weathered and Fractured basalt	6-98
Massive Basalt with scoria	98-108
Fractured basalt with gravel	108-134
Massive basalt with scoria	134-172
Weathered and Fractured Basalt	172-200
Basement(Gneiss)	200-

The resistivity value of the two upper parts ρ_1(2.7-5.6 Ohm-m) and ρ_2(30-100 Ohm-m) are correlated to the top black cotton soil and highly weathered and fractured basalt respectively. The second resistivity layer ρ_2(30-100 Ohm-m) which is found beneath L8-V1,L8-V2 and L8-V3 overlaid by the black cotton soil and underlain by the massive basalt with scoria might be a good sources of ground water at shallow depth up to 30m. Even if there is no data that shows successive water strike depth for borehole BTW7, it is hopefully expected within resistivity layers of $\rho_2, \rho_4,$ and ρ_6 due to low resistivity value of the layers and type and degree of weathering and fracturing of rocks found in this layers identified from BTW7 lithologic units. Therefore, in addition to ρ_2(30-100 Ohm-m) the two low resistivity layers; fractured basalt with gravel with resistivity ρ_4(25-75 Ohm-m) and highly weathered and fractured basalt with resistivity ρ_6(3-82.6 Ohm-m) are expected to be a good sources of groundwater. The upper part of the basement beneath L8-V3 and L8-V4 is also weathered and it can be considered as an aquifer together with the upper highly weathered and fractured basalt.

Generally, the resistivity of each layer decreases towards L8-V3 which is also shown in Figure 4.4. In the pseudodepth section of Line-8, it is shown as low apparent resistivity value to the pseudodepth of 1000m beneath L8-V3 and the drilled borehole around this place (BTW7) has ground water yield of greater than 5.6 l/sec.

The two structural lines observed in the case of qualitative interpretation (Figure 4.11) are also observed in this geoelectric section (Figure 4.12). Since the VES points has a minimum separation of 1 km and maximum separation of 2km, the orientation of these structures in the case of qualitative interpretation (Figure 4.11) and the distribution of apparent resistivity values in pseudodepth section of Line-8 (Figure 4.2) and the resistivity layer orientation in this geoelectric layer were considered to put them in the appropriate location.

B) Geo-electric section along Line-6(V1-V3)

The geo-electric section of Line six (Figure 4.13) was constructed from the model parameters of VES points data found along Line-6(V1-V3). The boreholes GW1 and GW2 located around L6-V3 and L6-V1 respectively were used to constrain depth and identify the lithologic units beneath these VES points during modeling. The lithologic data from the two boreholes and GW4 together with the resistivity parameters found from modeling of each VES point data were used to prepare the geoelectric section shown below (Figure 4.13). Table 4.3 below shows the lithologic log along Line six from the three boreholes (GW1, GW4 and GW2).

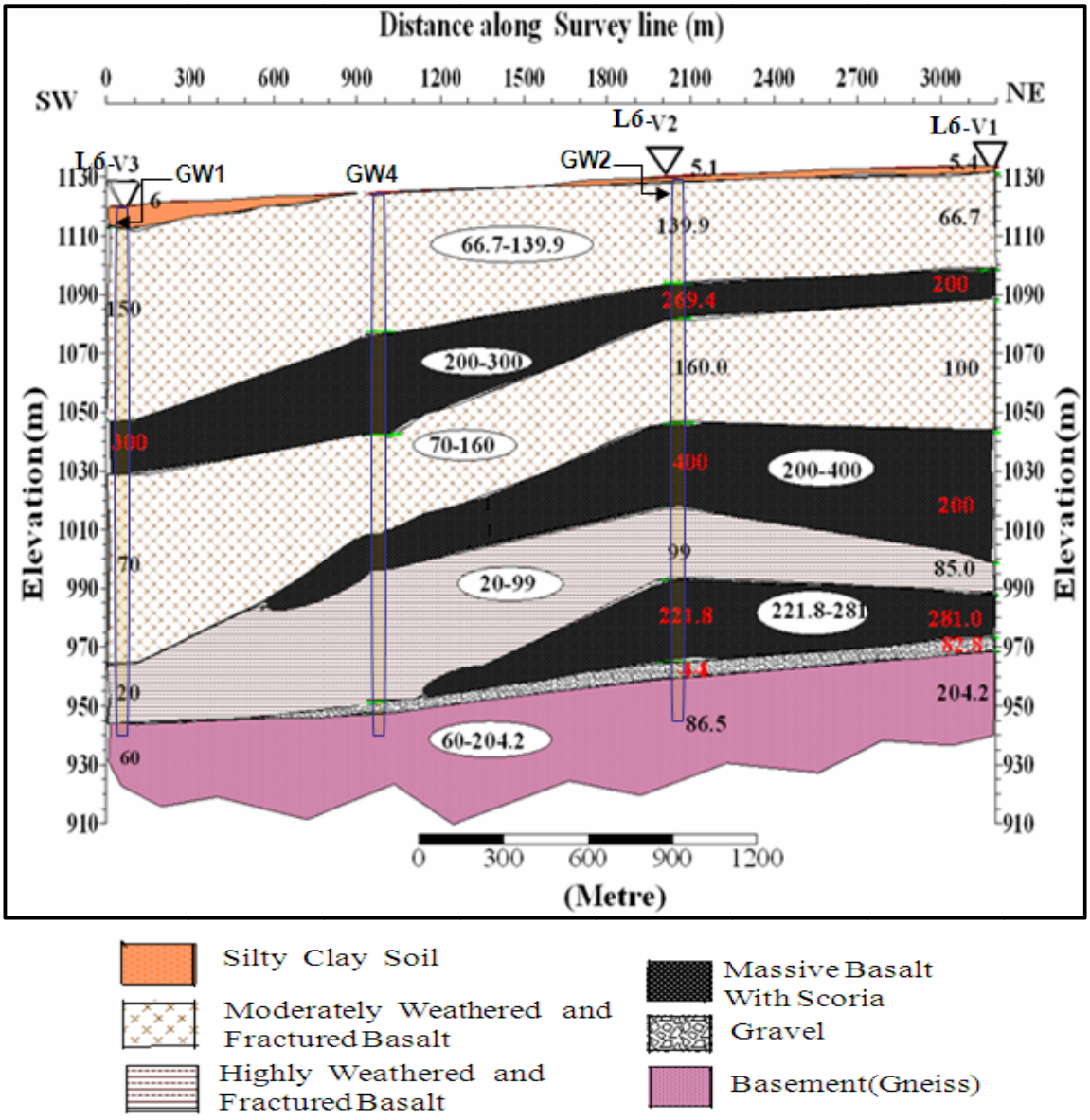

Figure 4.13 Geo-electric section along Line-6, Gelchet, Borena Zone.

The geoelectric section (Figure 4.13) show that the shallow subsurface lithologic units found along Line six which are represented by nine geoelectric layers. From these, five are major and four are minor (having small thickness) geoelectric units. The nine geoelectric units have relative resistivities in accordance with the following patterns;

$\rho_1 < \rho_2 < \rho_3 > \rho_4 < \rho_5 > \rho_6 < \rho_7 > \rho_8 < \rho_9$ from top to bottom. The four minor lithologic units with their resistivity values; ρ_1 (5-6 Ohm-m) found at the top is correlated to the Silty clay soil, ρ_8 (4.4-82.8 Ohm-m) found above the basement having maximum thickens value of 6m beneath L6-V1 is correlated to gravel, ρ_5 (200-400 Ohm-m) and ρ_7 (221-281 Ohm-m) which are found above the highly weathered and fractured layer and gravel respectively are correlated to massive basalt with scoria.

The thickens of ρ_1 (5-6 Ohm-m) shown beneath L6-V3 is 5m but this thickens decrease from L6-V2 towards L6-V1 and it is absent around GW4 which is found in between L6-V3 and L6-V2. This layer has low resistivity value due to its clay nature. The eighth resistivity layer with resistivity value ρ_8 (4.4-82.8 Ohm-m) has small thickens (0 to 6m) compared to the other units and disappears to the west of GW4. Being overlain by massive basalt with scoria and underline by basement (genies), it is good groundwater aquifer due to its high porosity and permeability nature.

The five major lithologic units with resistivity values ρ_2 (66.7-139.9 Ohm-m), ρ_3 (200-300 Ohm-m), ρ_4 (70-160 Ohm-m) , ρ_6 (20-99 Ohm-m) and ρ_9 (60-204.2 Ohm-m) are correlated to the moderately weathered and fractured basalt, moderately weathered and fractured basalt, highly weathered and fractured basalt and upper part of basement(gneiss) respectively. The fourth and six resistivity layers with thickness from 10-20m and 36-66m respectively are expected to be good sources of ground water which is also confirmed from the drilled boreholes as the range of water strike depths are found within these layers.

Generally, the resistivity of each layer decreases towards L6-V3 also shown in Figure 4.4 and beneath this VES point, the resistivity value for the layers are shown as low up to the basement. The drilled borehole (GW1) around L6-V3 has groundwater yield of greater than 17 l/sec whereas GW2 located near to L6-V2 has yield which is greater than 15 l/sec. As it is shown in the geoelectric section of Line six (Figure 4.13), an increase in thickens of the two resistivity

layers (ρ_4 & ρ_6), decrease in their resistivity values together with the upper part of basement, and decrease in the basement topography from L6-V2 towards L6-V3 leads to have GW1 high groundwater yield than GW2.

Table 4.2 Lithologic log of boreholes GW1, GW4 and GW2

Lithology	**Depth(m) from the surface**		
	GW1	GW4	GW2
Silty Clay Soil	0-4	-	0-2
Moderately weathered and fractured Basalt	4-72	0-48	2-42
Massive Basalt	72-90	48-82	42-54
Moderately weathered and Fractured Basalt	90-156	82-116	54-100
Massive Basalt with scoria	-	116-128	100-136
Highly weathered and Fractured Basalt	156-174	128-174	136-154
Massive basalt with scoria	-	-	154-168
Gravel	-	174-178	168-170
Basement(Gneiss)	174-	178-	170-

4.3.2 Gravity Modeled sections

Gravity modeling is usually the final step in gravity interpretation and involves trying to determine the density, depth and geometry of one or more subsurface bodies (Mickus, K., 2003). In this work, second degree polynomial surface fitting residual gravity anomaly data was used and the density contrast between the body of interest and the surrounding material was determined along two profiles by using forward modeling of 2.5D bodies. The lithologic unit and depth constraints for modeling were taken from geoelectric sections whereas the density ranges of these rocks were taken from Telford *et al* 1990. Several trials and successive improvements were conducted to get best fit between the calculated and observed anomalies

along the two profiles (Figure 4.14). The model was changed and the procedure was performed again until the match between the calculated values and the observed anomalies was deemed close enough. Since the gravity data has minimum separation of 300m and maximum separation of 1000m while the resistivity data has minimum separation of 1km and maximum separation of 2km, it is used to define clearly the causes of change in residual gravity anomaly observed in the qualitative maps. Unlike the resistivity method, the gravity data is not only caused by masses directly underneath but also by those found near or far away from the observation points. Moreover, the gravity measurement points are densely packed than the VES points with smaller sampling interval. Because of these, it has a great potential to model the subsurface horizontally in a continuous way, if the appropriate constraint is laid on the vertical direction.

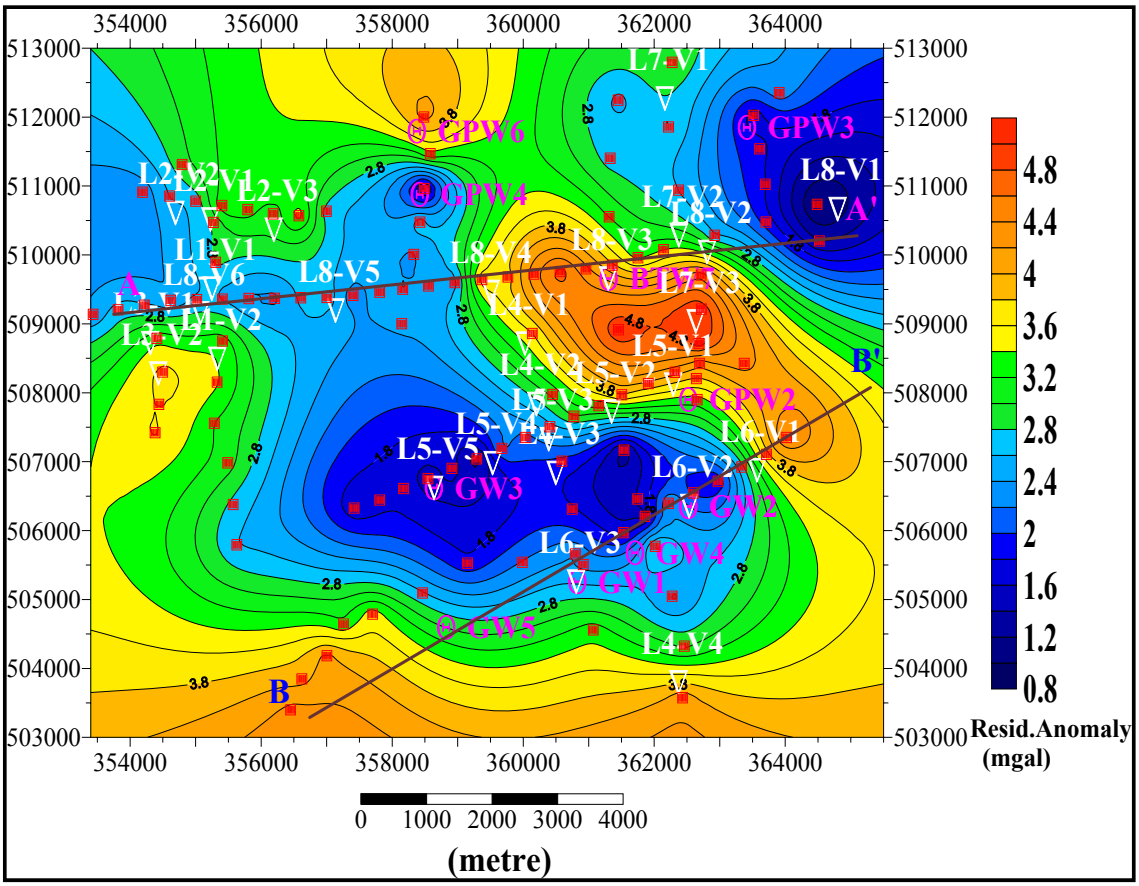

Figure 4.14 Modeled gravity profiles from second degree residual gravity anomaly map.

A) Gravity Modeled Section along profile AA'

The gravity modeled section along profile AA' (Figure 4.15) was produced from the gridded second degree residual gravity anomaly data. The modeled profile is oriented in the east-west direction with a total length of 11.30 Km. It includes the resistivity survey Line-8 with additional length to the west and east. The densities and thickens of the lithologic units which were identified in the geoelectric section of Line-8 are used to constrain the gravity model parameters at those points where there are information. The range of densities of these lithologic units were taken from Telford *et al* 1990 and the values were freely adjusted to fit the gravity data based on their degree of weathering , fracturing, type and depth of burial as shown in Table 4.3.

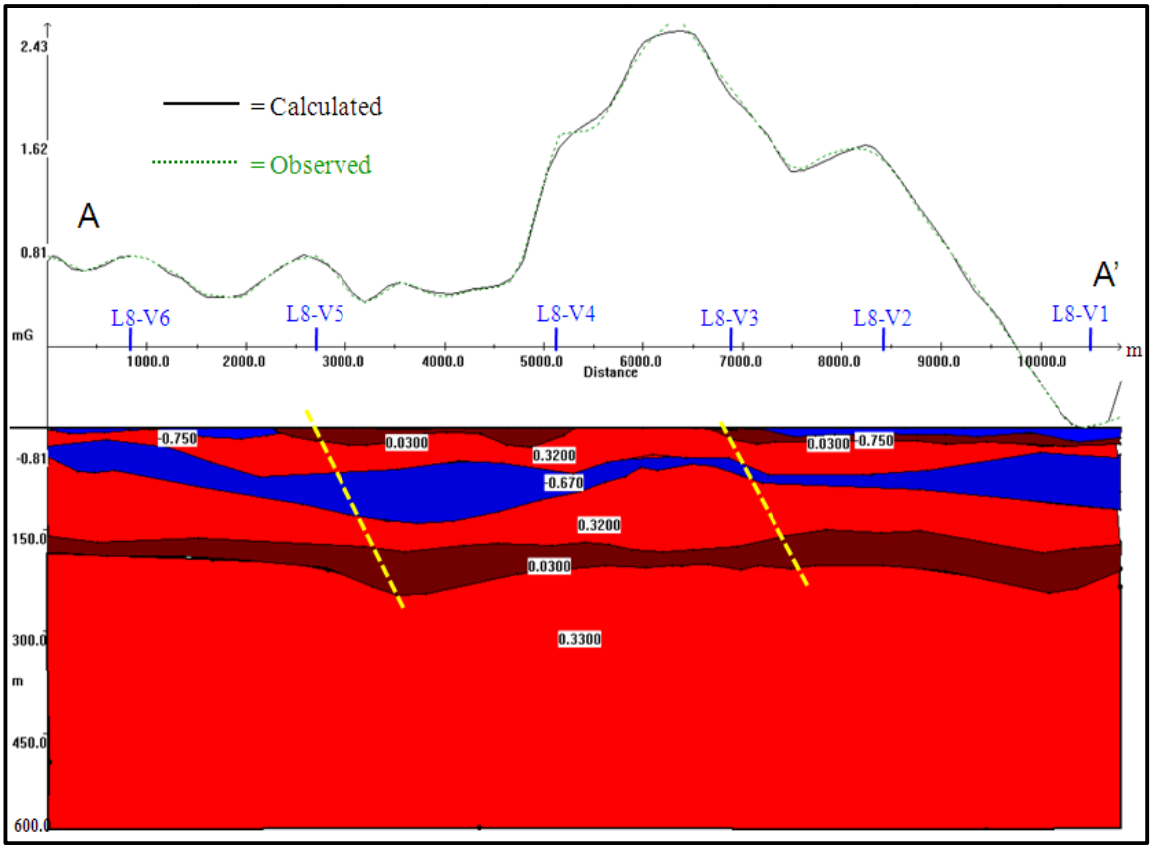

Figure 4.15 Gravity modeled section along profile AA'.

The modeling was performed by fitting the observed data with the calculated one by varying the geometry (depth and shape) on those places where we didn't have VES measurements. Where ever, we had VES measurements, depths of burial for lithologic units were fixed to VES results

and minimal adjustments were made to those depths. After several trials, the model shown in the Figure 4.15 which consists of five types of layers located at seven different places was obtained. Among these layers, the gneiss basement shown at the bottom has higher thickens and higher density value which is 3.0g/cm^3 as compared to the other layers found above it. The basement topography undulation along this profile is clearly seen together with the other layers. The depth to the gneiss basement along this profile varies from west to east within 184-245m range. The pick residual gravity value between L8-V4 and L8-V3 is caused by the thick (dens) basalt covers above the basement.

Table.4.3 Rock types and their density values used for modeling along profile AA'.

Rock Type	**Density Range (g/cm^3)**	**Average density (g/cm^3)**	**Density value used for modeling(g/cm^3)**	**Remark**
Black cotton soil	1.2-2.4	1.29	1.92	Average density of soil
Massive basalt	2.70-3.30	2.99	2.99	Average density of basalt
Fractured basalt with Gravel	1.7-2.4	2.0	2.0	Average density of gravel
Highly weathered and fractured basalt	2.7-3.30	2.99	2.7	The lowest density of basalt
Basement (Gneiss)	2.59-3.0	2.80	3.0	The highest density of gneiss

The thickens of the highly weathered and fractured layer found above the basement varies from 17m to 65m along this profile. This layer is shown as a low resistive layer in the geoelectric section of Line-8 and has high thickens in this modeled section where the basement has low topography whereas low thickens in places where the basement has high topography. Similarly,

the fractured basalt with gravel layer found in between the two massive basalt layers has maximum thickens in places where the basement topography is low whereas minimum thickens in places with high basement topography. The black cotton soil cover found in the east and west part of the profile above the weathered and fractured layer has a maximum thickens value of 15m and density of 1.92g/cm^3. This layer is not observed in the middle of the survey line where the massive basalt and weathered and fractured basalt are seen on the surface. The orientations of the two structural lines observed in the qualitative interpretation and geoelectric section of Line-8 are also shown in this gravity modeled section.

B) Gravity modeled section along profile BB'

The gravity modeled section along profile BB' (Figure 4.16) was produced from the gridded second degree residual gravity anomaly data. It has southwest-northeast orientation and a length of 9.718Km which includes the resistivity survey Line-6, but with further extended length. Similar to the modeled profile AA', the rock type and geometry (depth and shape) identified in the geoelectric section of Line-6 and their densities from Telford *et al* 1990 (Table 4.4) were used as a constraint for the gravity modeling. The modeling was performed by fixing the depth values to that of the VES results at those points where VES information were found and by freely adjusting at those points where VES data were not available. Later minor adjustments were made to the VES result to fit the modeled data with the measured one. After several trials, the model shown in the Figure 4.16, which consists of six different types of layers, was generated.

The basement topography undulates between 104m to 245m below the surface along this profile. It has low topography near to L6-V3 and L6-V2 whereas high topography to the east of L6-V1. Generally; the basement topography deceases from the southwest edge of the profile towards L6-V3 and increase from L6-V1 in the northeast direction but finally decrease to121m. The low topography basements are overlaid by the gravel layer which has a maximum thickens of 6m and didn't continue either to the southwest or northeast because it is bounded by the high topography basement from both sides. This is also true for the massive basalt layer, which is found above the gravel layer, but the other massive basalt layer found in between the highly weathered and fractured layer with density value of 2.7g/cm^3 and the moderately weathered and fractured layer with a density value of 2.8 g/cm^3 continues in the northeast direction up to the end of the survey line. The top Silty clay soil with density value of 1.92g/cm^3 covers the

southwest parts with an increase in thickness from L6-V3 to the southwest but thin out around the southwest end. This soil is also observed in the northeast of L6-V1 with very small thickens. The massive basalt layer that underlies the Silty clay soil and overlay the moderately weathered and fractured layer has a density of about 2.99g/cm^3 and thickens which vary from 20m to 100 m in the northeast to southwest direction. This layer is exposed on the surface around the southwest end of the profile.

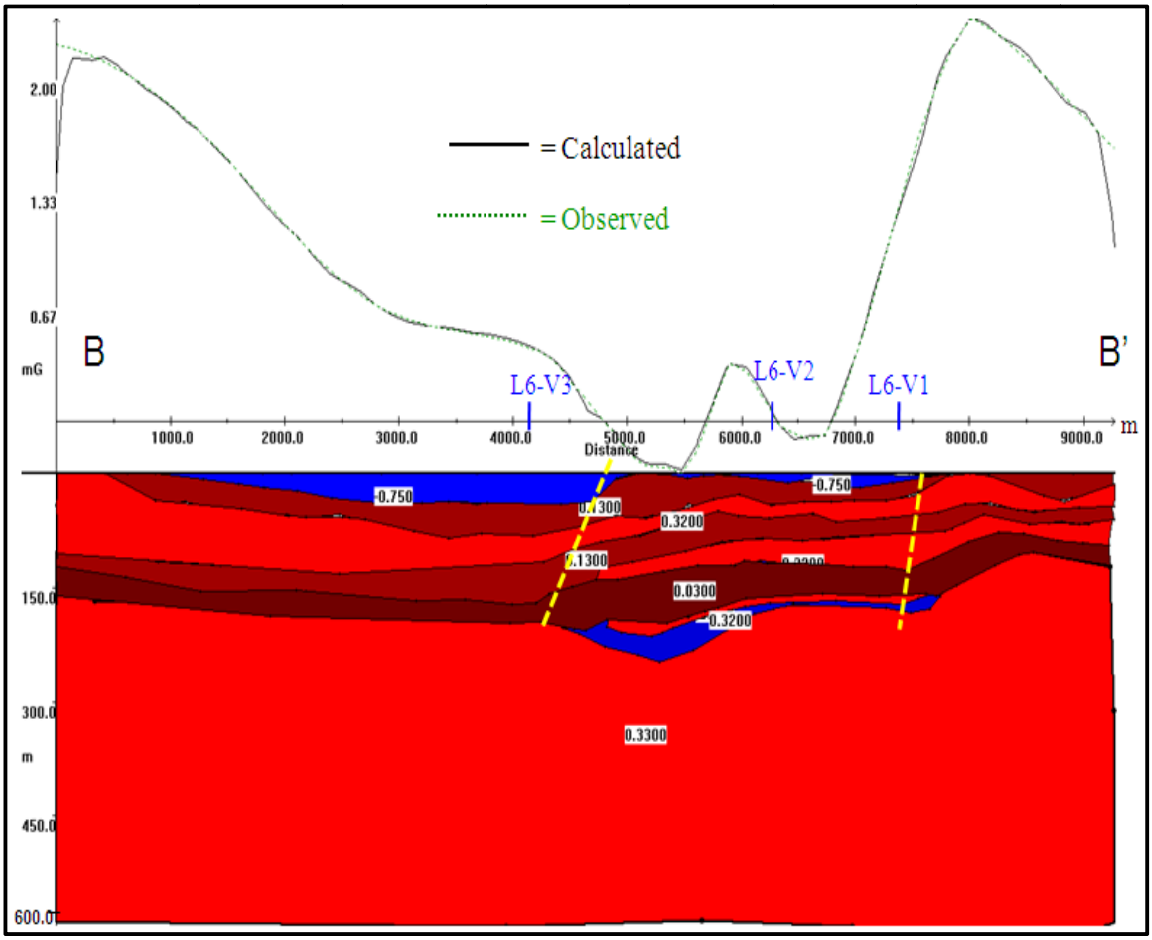

Figure 4.16 Gravity modeled section along profile BB'

The highly weathered and fractured layer that overlay the gravel and massive basalt layers beneath L6-V1 and L6-V2 in the northeast and the basement in the southwest end of the profile has a density of 2.7g/cm^3 and thickens value which varies from 20m to 70m. It is thick beneath the three VES points where the basement topography is low and lower thickens value where the basement topography is high. The two moderately weathered and fractured layers found beneath the top Silty clay soil and above the highly weathered and fractured layer have density value

that amount to 2.8g/cm^3. The thickens of the layer that underlain the Silty Clay varies from 10m to 52m whereas the thickens of the layer that overlay the highly weathered and fractured basalt varies from 14m to 54m. The former of this two layer disappears at the southwest end of the profile but have higher thickens beneath L6-V2 and to the southwest of L6-V3. The latter, which is moderately weathered and fractured layer has maximum thickens in southwest of L6-V3 and to the northeast of L6-V1. The orientations of two structural lines observed in the qualitative interpretation are also shown in this gravity modeled section.

Table.4.4 Rock types and their density values used for modeling along profile BB'.

Rock Type	**Density Range (g/cm^3)**	**Average density (g/cm^3)**	**Density value used for modeling(g/cm^3)**	**Remark**
Silty Clay Soil	1.2-2.4	1.92	1.92	Average density of soil
Moderately weathered and fractured Basal	2.70-3.30	2.99	2.8	greater than the lowest density of basalt
Massive basalt	2.70-3.30	2.99	2.99	Average density of basalt
Highly weathered and fractured basalt	2.7-3.30	2.99	2.7	The lowest density of basalt
Gravel	1.7-2.4	2.0	2.0	Average density of gravel
Basement (Gneiss)	2.59-3.0	2.80	3.0	The highest density of gneiss

CHAPTER FIVE

CONCLUSION AND RECOMMENDATION

5.1 Conclusion

This work presented the results of integrated geophysical survey that was conducted in the Borena Zone of Oromia Regional State, Southern Ethiopia with the aim to investigate groundwater potential zones and map possible structures, which serves as a conduit for groundwater movement. A total of 28 VES and 115 gravity points were visited to gather data. The gravity survey was accompanied by DGPS survey. The data were carefully collected, processed and interpreted. The interpretations were made qualitatively as well as quantitatively to achieve the desired objectives.

The qualitative interpretation of the VES data were performed by preparing apparent resistivity plan maps and pseudodepth sections whereas the interpretation of the gravity data were made based on the second degree residual gravity profile plots and gravity anomaly maps. The quantitative interpretation of VES data were made using geoelectric section along two selected profiles constructed using parameters which are derived from the inversion of VES data found on these profiles. The interpretation helped to identify different lithologic units. On the other hand, the quantitative interpretation of gravity data was performed by using forward modeling of the second degree residual gravity anomaly data along two selected profiles. The main aim of the gravity survey was to map the basement topography, geological structures and different layers in areas where VES information was not available. Especial focus was given in the mapping of the basement undulation.

There are test boreholes and other boreholes drilled as a result of this work in the study area. The comparison of the geophysical interpretations with drilled borehole results shows that the results of the integrated geophysical survey are in a very good agreement with the borehole logging results. The comparison of well yield with the geophysical survey results demonstrated the capacity of using resistivity (VES) and gravity surveys for demarcating groundwater potential zones, especially in diverse geological setup which are composed of volcanic rocks in the metamorphic terrains.

From the results, discussion and interpretation of this study, the following conclusions have been forwarded:

1) The qualitative interpretations resulted in identifying four weak zones. Two of these weak zones are faults. The two fault and one of the weak zone lines were named and surfecially mapped by previous geological work. On the other hand, the fourth weak zone that passes through L2-V2 in the northwest-southeast direction was not mapped by previous geological work rather from this geophysical work. The first fault line starts from the central part in the north and extends in the southwest direction by crossing Line eight near to L8-V5. The second fault line runs from the northern part of the area near to the first fault line and extends to the south-east until it encounter the massive basalt in the central-eastern part of the area. Finally, it continues to L6-V1 in the southeast direction. The third fracture runs from the southwestern part of the area toward east and terminates near L6-V3. The gravity model along BB' near to L6-V3 shows that this fracture is a fault.

2) It is believed that the groundwater flows using these structures and fractures of lithologic units to accumulate over the basement wherever the basement has bowl like shape or depression. Therefore, whenever fault lines, fractures and low basement topography are interpreted and accompanied by low resistivity values at higher depths, these places are identified as good groundwater potential zones. As a result of the above, the place where GW3 was recommended has low basement topography and the lowest resistivity value at higher depth and hence identified as the most favorable place for drilling. Even if GPW4 and GPW6 were drilled near to the fault line one and two, these places are located at high resistivity value zones up to higher depth and on relatively higher basement topography. As a result of this, these boreholes haven't produced water.

3) The geoelectric sections show that the area has four main types of lithologic units which differ in different degree of weathering, level of fracturing, composition, thickens and depths of burial. These are correlated with quaternary vesicular basalts, gravel (with weathered and fractured vesicular basalts), massive basalt with scoria and basement (gneiss). In some places, the top layer is covered by silty clay soil or black cotton soil with very small thickness. The test drilling results carried out

before this work and those drillings as a result of this work shows the layers that directly overlain the upper part of the basement are mostly weathered and fractured relative to the other layers and are good aquifers depending on their location in relative to structures and basement topography. The gravel and the weathered and fractured vesicular basalts are good groundwater bearing horizons, especially in places where structures are accompanied by low basement topography.

4) The gravity modeling along the two lines revealed that depth to the basement varies from125m to 245m along profile AA'and from 104m to 245m along profile BB'. The densities of the different layers namely top silty clay (black cotton) soil, moderately weathered and fractured basalts, highly weathered and fractured basalt, massive basalt, gravel (with weathered and fractured vesicular basalts) and the gneiss basement are given by 1.92, 2.8, 2.7, 2.99, 2.0 and 3.0g/cm^3 respectively.

In general, the integrated geophysical survey that was carried out in this work is successful in mapping structures and the basement topography, which serves as conduit for groundwater movement and a place where it accumulate respectively. The work has not only demonstrated the advantage of using integrated geophysical survey for groundwater exploration but also proved the importance of using methods such as high precision gravity survey which have to be considered as a secondary technique in groundwater exploration.

5.2 Recommendation

Based on the outcome of this study, the following are recommended.

1) The aquifer system of the area is controlled by the structural lines and the basement topography so that drilling is recommended to be done at places having low resistivity at large AB/2 separation, low basement topography as deducted from gravity survey and where the structural futures such as faults are encountering massive basalts or where they terminate. Even if there are ten already drilled boreholes (some of them are recommended as a result of this work) in the study area, depending on the need and necessity of the pastoralist and nomadic people, the following two boreholes are recommended for drilling in the following order. The first borehole is recommended to the south of GW3 and north of GW5 with UTM

coordinates (359420, 505441, 1120) and the second borehole in the northwestern part of the study area near to L2-V2 with coordinate (354691, 510609, 1060).

2) Additional Vertical Electrical Sounding survey is recommended in the northwestern part of the area to examine the extension of low resistivity zones.

3) Similar detailed gravity survey outside of the area is recommended to know the extension of faults that are behaved to served as conduit for groundwater flow and to study the extension of the promising low gravity and low resistivity zone in the northwest part of the area.

4) Detailed structural geological investigations are recommended to study the density and orientation of weak zones as well as their natures such as dip, strike and their extension.

5) Further regional hydrological and hydrogeological investigations are recommended to understand the basin, amount of precipitation and evaporation which are used to estimate the percolation of surface water to the groundwater.

REFERENCES

Abebe, E., 2010; *Geodetic determination of plate velocity vector in the Ethiopian rift.* M.Sc. thesis (unpublished), Department of Earth Sciences, Addis Ababa University, Addis Ababa, Ethiopia.

Alemayehu, T., 2006; *Groundwater occurrence in Ethiopia.* Addis Ababa University, Addis Ababa, Ethiopia.

Awoke, H. and Hailu, F.(compilers), 2007; *The geology of yabelo map sheet (NB 37-14).*Geological survey of Ethiopia, Regional Geology and Geochemistry department, Addis Ababa, Ethiopia.

Becker, M., 1984; *Analyse von hochpraezisen Schweremessungen.* Dissertationen, Deutsche Geodaetische Kommission, Reihe C, Nr. 294, Muenchen, Germany**.**

Belete, Y., Abaire, B., Asefaw, B., Tigabe, M., Shiferaw, D., Belachew, M., Adege, N., Mulachew, A. and Abdela, M., 2000; *Hydrogeological, Geophysical and Engineering geological investigation of yabelo map sheet (NB 37-14*). Ministry of Mine and Energy, Ethiopian Institute of Geological Surveys, Hydrogeology, Engineering geology and Geothermal department, Addis Ababa, Ethiopia.

Blakely, J.R., 1996; *Potential theory in gravity and magnetic applications. Cambridge University press*, Cambridge, UK. Pp 43-63,128-154.

Dobrin, M.B. and Savit, C. H., 1988; *Introduction to geophysical prospecting, fourth edition.* McGraw-Hill, New York, USA .Pp498-613,750-837.

Fetter, C.W., 2001; *Applied Hydrogeology,4th Edition*. Prentice-Hall, Inc. London, UK. Pp 1-20.

Gibson, P.J.and George, D.M., 2003; *Environmental applications of geophysical surveying techniques.* Nova Science Publishers, Inc. New York, USA .Pp45-49,137-177.

Kazmin, V., 1972; *Geology of Ethiopia, Explanatory notes to geological map of Ethiopia.* Ethiopian Institute of Geological surveys, Addis Ababa, Ethiopia.

Kearey, P., Brooks, M. and Hill, I., 2002; *An Introduction to Geophysical Exploration, third edition.* Blackwell Science Ltd. Oxford, UK .Pp 125-153,183-196.

Kirsch, R., 2006; *Groundwater Geophysics. A Tool for Hydrogeology.* Springer-Verlag Berlin Heidelberg, Germany.

Lacoste and Romberg, 2003; *Lacoste and Romberg Aliod 100 upgrade user's manual.* Lacoste and Romberg lnc. Austin, USA.Pp2-16.

Ledo, L., 2007; *Hydrogeophysics as a multidisciplinary tool on aquifer Appraisal: focus on AMT capabilities.* PhD thesis, Universidad de Barcelona, Spain. Pp3-25.

Lewi, E., 1997; *Modeling and inversion of High Precision Gravity Data. Dissertationen,Deutsche Geodaetische Kommission, Reihe C, Nr. 471, Muenchen, Germany.*

Li, X. and G¨otze, H., 2001; *Tutorial Ellipsoid, geoid, gravity, geodesy, and geophysics.* Journal of Society of Exploration Geophysicists. Geophysics, Vol. 66, NO. 6. Pp 1660-1668.

Mickus, K., 2003; *Gravity method: environmental and engineering applications.* Department of Geosciences, Southwest Missouri State University, Springfield, MO 65804; Pp1-10.

Moritz, H., 2000; Geodetic *reference system 1980.In:C.C.Tschering(ed), the Geodesist's hand book 1984-Bulletin Géodésique .Pp58, 388-398.*

OWWDSE, 2008; *Detailed* reconnaissance *geological study of Borena zone, Borena groundwater study project geology report.* Oromia water works, Design and supervision enterprises, Addis Ababa, Ethiopia. Pp1-50.

Parasnis, D.S., 1962: *principle of applied geophysics, 3rd edition*. Chapman and hall, London, England. Pp 59-96, 98-129.

Reynolds, J.M., 1997; *An Introduction to Applied and Environmental Geophysics.* John Wiley and Sons limited, England, UK. Pp 29-116,415-522.

Robinson, E.S., and Caruh, C., 1988; *Basic exploration geophysics*. John Wiley and Sons Limited, New York, USA. Pp 221-324.

Sultan, A. Mekhemer, M. Santos, M. and Abdi Alla, M., 2009: *Geophysical measurements for subsurface mapping and groundwater exploration at the central part of the Sinia peninsula, Egypt.* The Arabian journal for science and Engineering, volume 34, Number1a. Pp103-118.

Taylor, J.R., 1997; *An introduction to Error Analysis. The study of Uncertainties in physical measurements, second edition*. University sciences Books, Sausalito, California, USA.Pp45-79.

Telford, W.M., Geldart, L.P. and Sheriff, R.E., 1990; *Applied Geophysics, 2nd Edition*. Cambridge University Press, Cambridge, UK. Pp 6-48,522-562.

Wikipedia, 2011; *Geoid.Answers.com.Wikipedia*.
http://www.answers.com/topic/geoid, accessed January 12, 2011.

ANNEX

MODELED VES CURVES

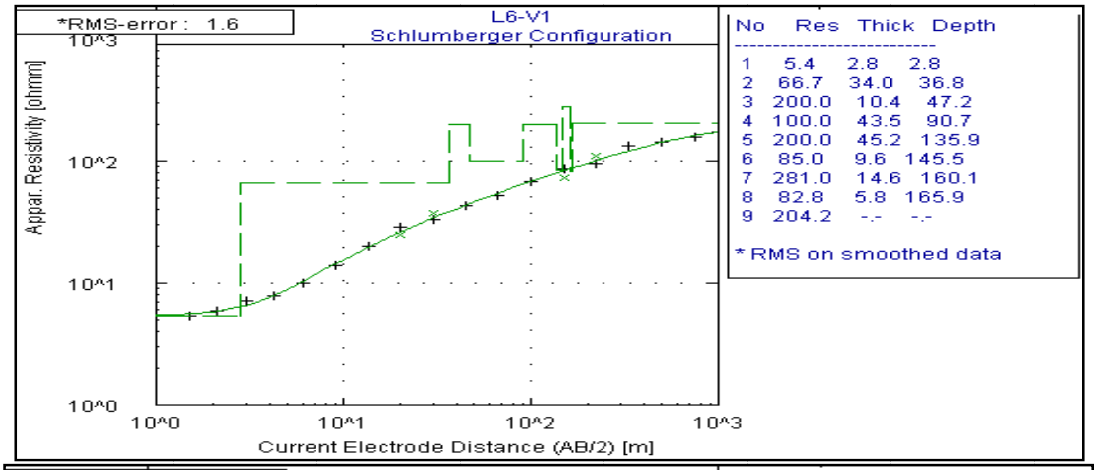

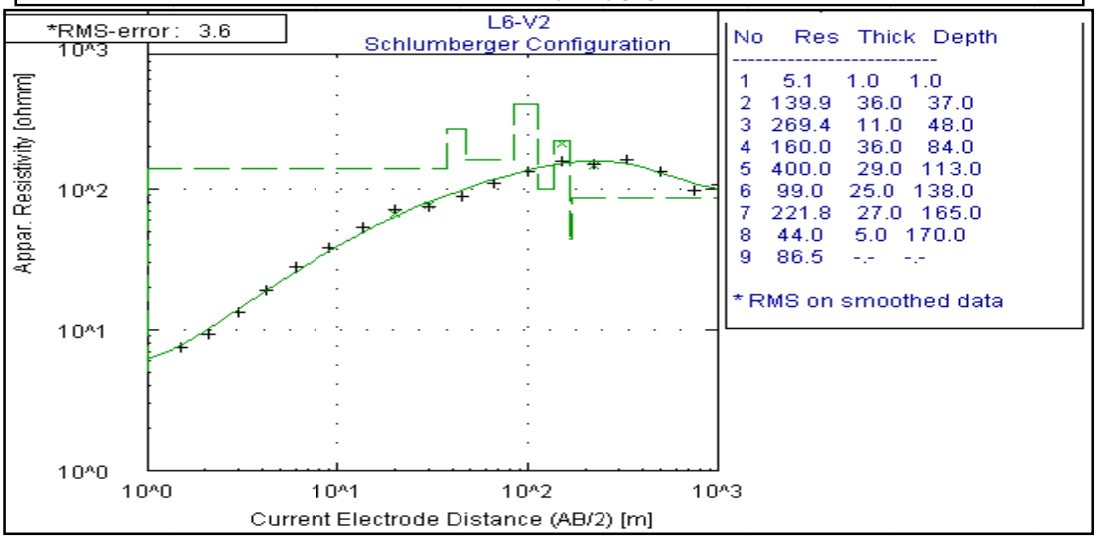

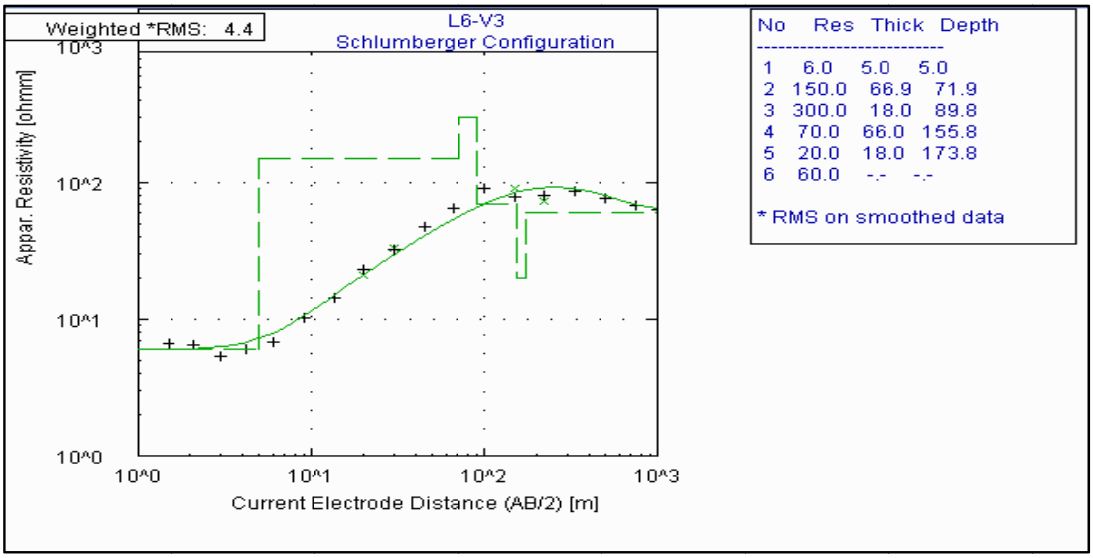

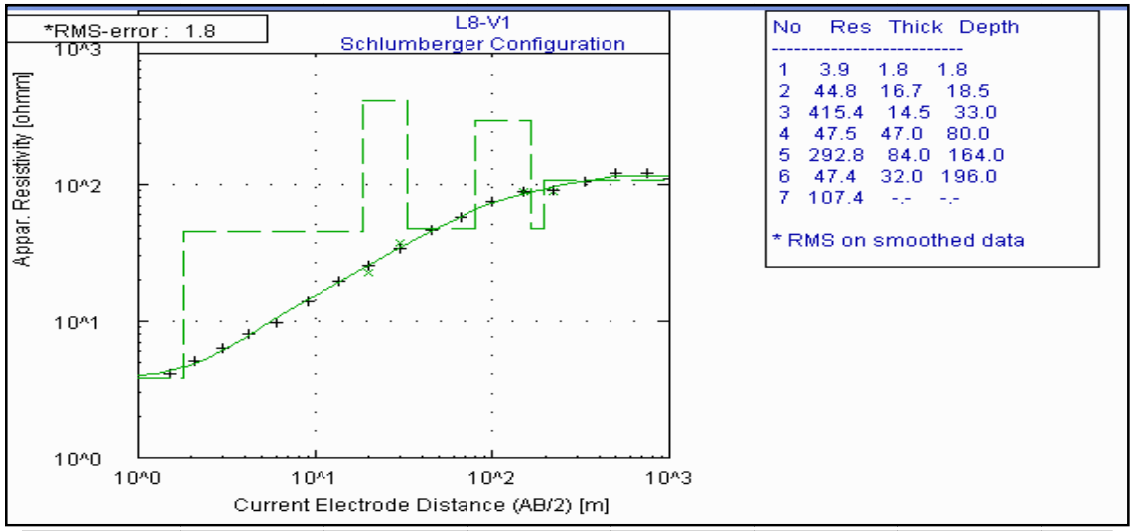

No	Res	Thick	Depth
1	3.9	1.8	1.8
2	44.8	16.7	18.5
3	415.4	14.5	33.0
4	47.5	47.0	80.0
5	292.8	84.0	164.0
6	47.4	32.0	196.0
7	107.4	-.-	-.-

* RMS on smoothed data

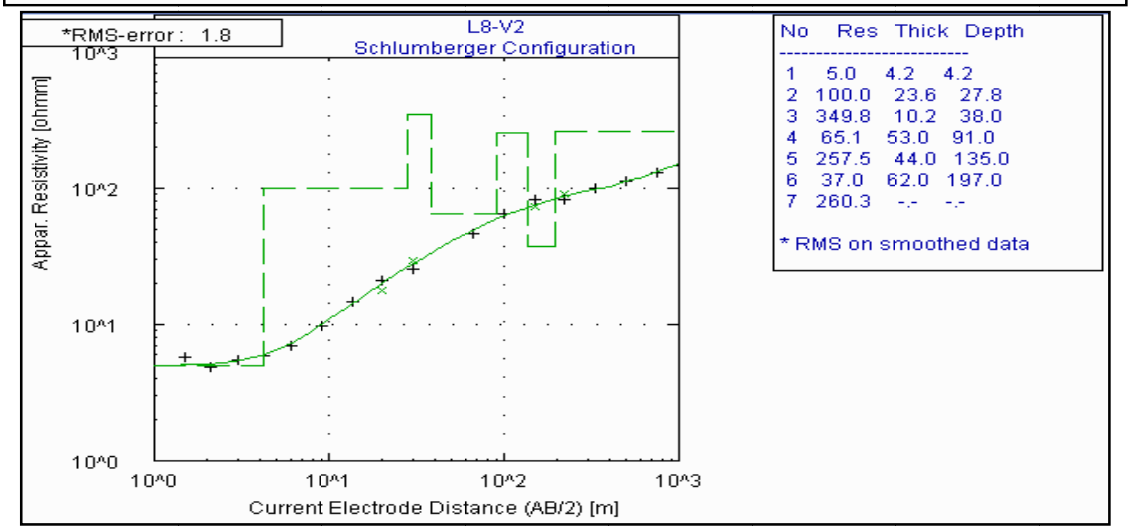

No	Res	Thick	Depth
1	5.0	4.2	4.2
2	100.0	23.6	27.8
3	349.8	10.2	38.0
4	65.1	53.0	91.0
5	257.5	44.0	135.0
6	37.0	62.0	197.0
7	260.3	-.-	-.-

* RMS on smoothed data

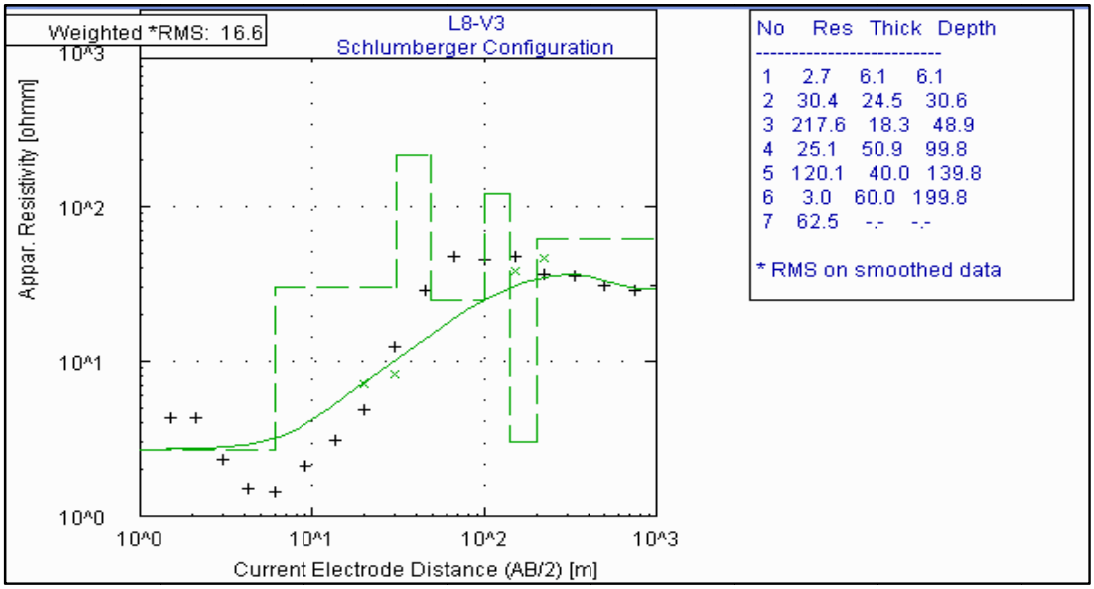

No	Res	Thick	Depth
1	2.7	6.1	6.1
2	30.4	24.5	30.6
3	217.6	18.3	48.9
4	25.1	50.9	99.8
5	120.1	40.0	139.8
6	3.0	60.0	199.8
7	62.5	-.-	-.-

* RMS on smoothed data

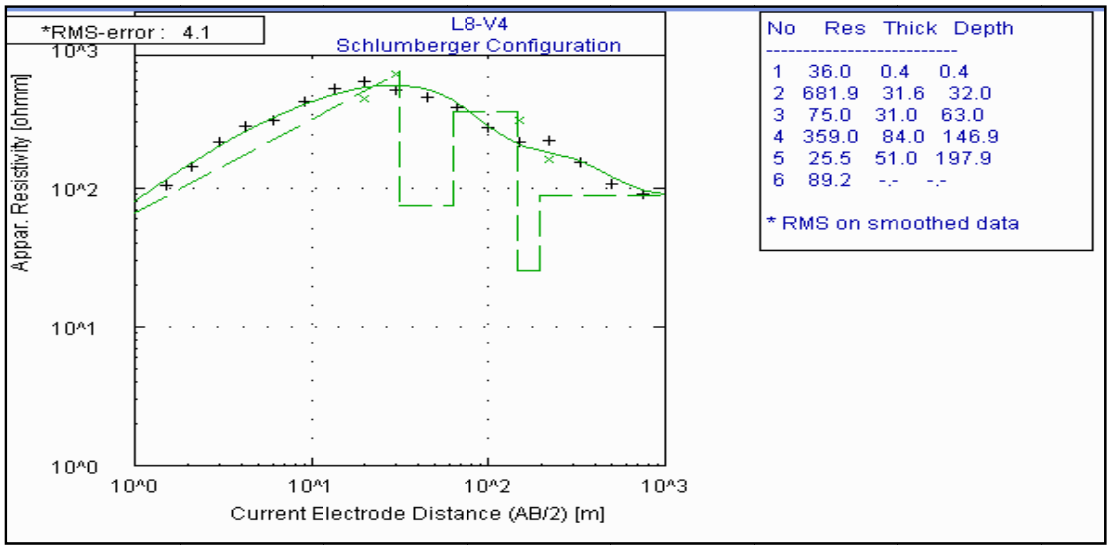
*RMS-error : 4.1
L8-V4
Schlumberger Configuration
Appar. Resistivity [ohmm]
10^3
10^2
10^1
10^0
10^0
10^1
10^2
10^3
Current Electrode Distance (AB/2) [m]
No Res Thick Depth
1 36.0 0.4 0.4
2 681.9 31.6 32.0
3 75.0 31.0 63.0
4 359.0 84.0 146.9
5 25.5 51.0 197.9
6 89.2 -.- -.-
* RMS on smoothed data

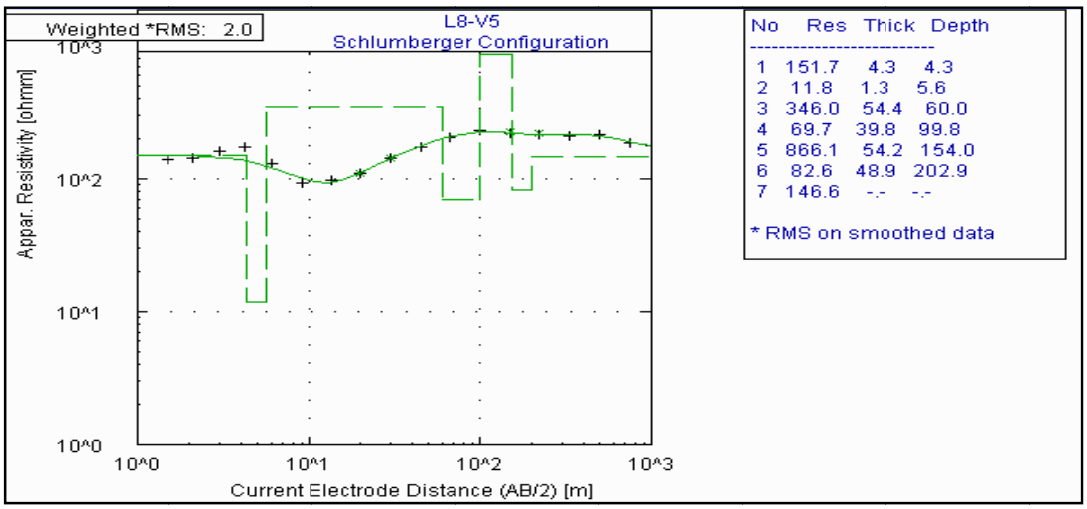
Weighted *RMS: 2.0
L8-V5
Schlumberger Configuration
Appar. Resistivity [ohmm]
10^3
10^2
10^1
10^0
10^0
10^1
10^2
10^3
Current Electrode Distance (AB/2) [m]
No Res Thick Depth
1 151.7 4.3 4.3
2 11.8 1.3 5.6
3 346.0 54.4 60.0
4 69.7 39.8 99.8
5 866.1 54.2 154.0
6 82.6 48.9 202.9
7 146.6 -.- -.-
* RMS on smoothed data

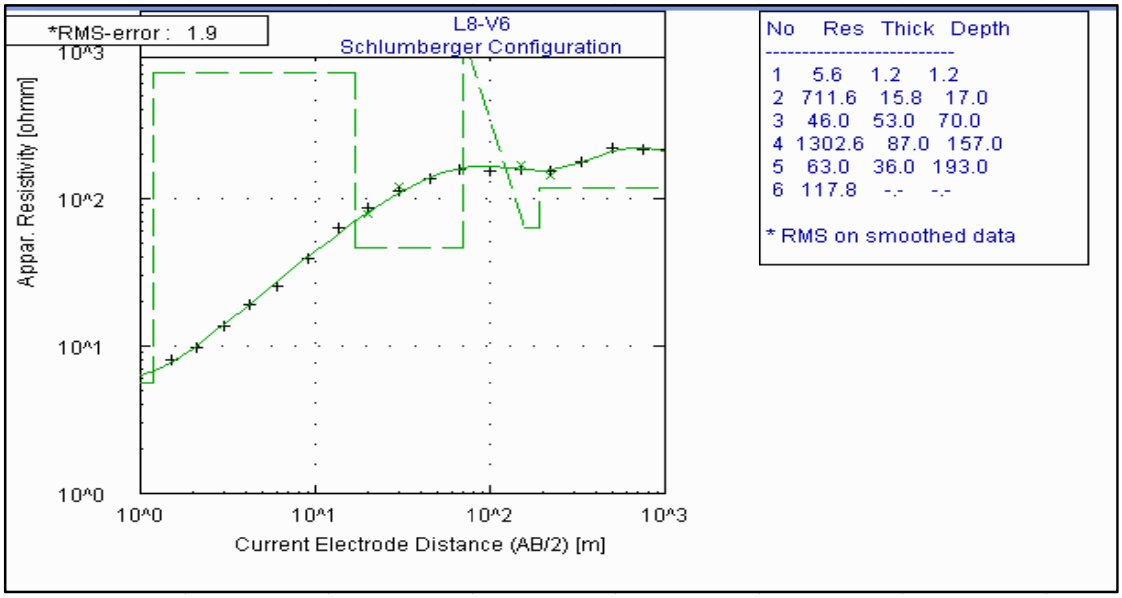
*RMS-error : 1.9
L8-V6
Schlumberger Configuration
Appar. Resistivity [ohmm]
10^3
10^2
10^1
10^0
10^0
10^1
10^2
10^3
Current Electrode Distance (AB/2) [m]
No Res Thick Depth
1 5.6 1.2 1.2
2 711.6 15.8 17.0
3 46.0 53.0 70.0
4 1302.6 87.0 157.0
5 63.0 36.0 193.0
6 117.8 -.- -.-
* RMS on smoothed data

Declaration

This thesis is my original work and has not been presented for degrees in any other University and all sources of materials used for the thesis have been duly acknowledged.

Mulugeta Chanie Fenta Signature_____ Date_____

Dr.Elias Lewi (Advisor) Signature_____ Date_____

Dr.Tigistu Haile (Co-advisor) Signature_____ Date_____

February, 2011
Addis Ababa